SCIENCE CHINA
Earth Sciences

•RESEARCH PAPER•

August 2022 Vol.65 No.8: 1568–1585
https://doi.org/10.1007/s11430-021-9935-5

Neoarchean granitic rocks from the Jiamiao area of the Dabie orogen: Implications on the formation and early evolution of the Yangtze Craton

Yang TIAN[1,2,3], Wei WANG[2,3*], Wei JIN[1,4], Yuanbao WU[2], Jing WANG[1], Xin DENG[1,3] & Sifang HUANG[2,5]

[1] *Wuhan Center of Geological Survey, China Geological Survey, Wuhan 430205, China;*
[2] *State Key Laboratory of Geological Processes and Mineral Resources, School of Earth Sciences, China University of Geosciences, Wuhan 430074, China;*
[3] *Research Center for Petrogenesis and Mineralization of Granitoid Rocks, China Geological Survey, Wuhan 430205, China;*
[4] *Institute of Geology, Chinese Academy of Geological Sciences, Beijing 100037, China;*
[5] *Department of Surveying and Planning, Shangqiu Normal University, Shangqiu 476000, China*

Received November 25, 2021; revised March 21, 2022; accepted April 12, 2022; published online July 12, 2022

Abstract Archean rock exposures in the Yangtze Craton of South China are scarce and have been only studied in small-scale outcrops for understanding its early crustal evolution. Geological investigations have been carried out for three Neoarchean gneissic granitic plutons from the Dabie orogen in the northeastern margin of the Yangtze Craton. Zircon U-Pb geochronology constrains the emplacement of high-K monzogranite at 2645±30 Ma, high-K syenogranite at 2630±37 Ma and Na-rich granodiorite at 2497±29 Ma. These findings provide direct evidence for the existence of ~2.7–2.5 Ga rocks in the Dabie orogen, which significantly contribute to the distribution and evolution of Neoarchean basement rocks in the Yangtze Craton. Zircon crystals from the three granite samples give $\varepsilon_{Hf}(t)$ values of −0.9 to 3.7, −4.2 to −0.4 and −4.7 to 0.1, respectively, corresponding to T_{DM2} ages of 3186–2909, 3372–3141 and 3297–3005 Ma. The magmatic zircons have $\delta^{18}O$ values of 5.06±0.27‰ to 5.79 ±0.30‰ (average 5.59‰), 6.14±0.24 to 7.35±0.26‰ (average 6.87‰) and 5.95±0.17‰ to 7.09±0.17‰ (average 6.55‰), respectively. Considering the possible decrease of $\delta^{18}O$ value due to the lead loss during post-crystallization alteration, the primary $\delta^{18}O$ values might be substantially higher than those of the normal mantle zircon value ($\delta^{18}O$=5.3±0.6‰). These isotopic data indicate that the Jiamiao Neoarchean granites were largely generated through reworking of Paleo-Mesoarchean basement rocks with a minor contribution of supracrustal material. Integrating our findings with previous results, we infer that the Archean-Paleoproterozoic complexes/terranes of the Yangtze Craton have distinct petrogenesis and the timings of the transition from Na-rich to high-K granites, crustal growth, and tectonothermal evolution before ~2.0 Ga. However, all of them underwent metamorphism at about 2.0 Ga. These observations also reveal that the Yangtze Craton might comprise several microcontinents that evolved individually and collided to form a unified craton at ~2.0 Ga, synchronous with the assembly of the Columbia supercontinent. However, the lack of relevant data from the southeastern Yangtze Craton may have a critical influence on this conclusion and should be solved in the future.

Keywords Zircon U-Pb age, Hf-O isotopes, Neoarchean, Dabie orogen, Yangtze Craton

Citation: Tian Y, Wang W, Jin W, Wu Y, Wang J, Deng X, Huang S. 2022. Neoarchean granitic rocks from the Jiamiao area of the Dabie orogen: Implications on the formation and early evolution of the Yangtze Craton. Science China Earth Sciences, 65(8): 1568–1585, https://doi.org/10.1007/s11430-021-9935-5

* Corresponding author (email: wwz@cug.edu.cn)

1. Introduction

Archean crystalline basement rocks are crucial in investigating the formation and evolution of the continental crust, and have attracted substantial attention (Gao et al., 1999; Griffin et al., 2004; Zhang and Zheng, 2007; Wang et al., 2017; Wang K et al., 2018; Satkoski et al., 2017; Li et al., 2018; Maruyama et al., 2018). In contrast to the abundant outcrops of Archean basement rocks in the North China Craton, Archean basement exposures in the Yangtze Craton of South China are scarce, largely due to extensive sedimentary cover and superposition by later geological events. Some recent studies have indicated a widespread Archean crystalline basement in the Yangtze Craton (Liu et al., 2004; Zheng and Zhang, 2007; Ling et al., 2010; Guo et al., 2015; Zhao et al., 2019), however, a majority of the chronological evidence come from detrital or inherited zircons (Zhang et al., 2006b; Zheng et al., 2006; Liu X M et al., 2008; Han et al., 2017a; Wang W et al., 2018; Liu et al., 2021). Archean-early Paleoproterozoic rocks in the northern Yangtze Craton have been reported in sporadic complexes like the Kongling (Qiu et al., 2000; Zhang and Zheng, 2007; Jiao et al., 2009; Gao et al., 2011; Guo et al., 2015), Zhongxiang (Zhou et al., 2015; Wang Z et al., 2018; Huang et al., 2020), Yudongzi (Hui et al., 2017; Chen et al., 2019), and Feidong (Tu et al., 2021), while a few small outcrops have been reported at Cuoke (Zhao et al., 2020; Cui et al., 2020a) and Phan Si Pan (Zhao et al., 2019) in the southwest (Figure 1a).

The Dabie orogen in the northeastern Yangtze Craton, formed through the collision/subduction between South China and North China blocks in the Triassic, is one of the largest and best-preserved high- to ultrahigh-pressure metamorphic terrains in the world and is a key region for studying continent-continent collision geodynamics (Liou et al., 2009; Zheng, 2012; Zheng et al., 2019). The continental collision would tilt the whole crust and exposure ancient basement rocks to the surface, thus providing an opportunity for revealing the early Precambrian crustal evolution of the northern Yangtze Craton. However, Archean-Paleoproterozoic basement in the Dabie orogen has mainly indirectly been reported on the basis of xenocrystic or inherited zircons from metamorphic rocks like the Huangtuling granulite (Wu et al., 2002, 2008; Lei and Wu, 2008) and gneiss (Xia et al., 2003), Tuanfeng migmatite (Qiu et al., 2020), Muzidian gneiss (Qiu et al., 2021a) and the Xishui gneiss (Zhao et al., 2021) (Figure 1a). The age data from these rocks indicate a potentially widespread Archean-Paleoproterozoic crystalline basement, however, the ages obtained from xenocrystic or inherited zircon grains hamper a detailed understanding of the nature and composition of the crystalline basement. Therefore, identifying the Archean crystalline basement outcrop in the Dabie orogen is of great importance in constraining the formation and evolution of the continental crust in the Dabie orogen of the northeastern or even the whole Yangtze Craton.

This study provides the first report of three Neoarchean granite bodies from the Jiamiao area in the northern part of the Dabie orogen, based on geological mapping (1:50,000), field observation, and zircon LA-ICP-MS U-Pb dating. These Archean rocks provide vital information for evaluating the early crustal evolution of the Yangtze Craton. Representative samples were collected for petrography, geochemistry, geochronology, and zircon Hf-O isotope study to constrain their petrogenesis and tectonic evolution. The new data, in combination with the published results from other parts of the Yangtze Craton, provide valuable insights into its crustal accretion and evolution.

2. Geological setting

As the eastward extension of the Qinling Orogenic Belt in central China, the Dabie orogen can be subdivided into two segments from west to east, separated by the NNE-trending Shangcheng-Macheng Fault (Figure 1b and 1c). Based on the grade of metamorphism, the Dabie orogen can be subdivided into five tectonic units from north to south, comprising the Beihuaiyang (BHZ) greenschist-facies zone, the Northern Dabie (NDZ) high temperature (HT)/ultrahigh pressure (UHP) eclogite-facies zone, the Central Dabie (CDZ) medium temperature (MT)/ultrahigh pressure eclogite-facies zone, the Southern Dabie (SDZ) low temperature (LT)/ultrahigh pressure eclogite-facies zone, and the Susong (SSZ) low temperature and high pressure (HP) blueschist facies zone (Figure 1c) (Zheng et al., 2005). The NDZ is located between the Xiaotian-Mozitan and the Wuhe-Shuihou faults and mainly consists of Neoproterozoic grey granitic gneisses and Cretaceous granites, with sporadic meta-supracrustal rocks and UHP metamorphic rocks (Figure 1c). There are two migmatite domes, namely the Yuexi Dome in the east and the Luotian Dome in the west. Both the domes have similar lithologies and structures, with metamorphic grades ranging from granulite-facies in the core to amphibolite-facies at the margin wherein Mesozoic migmatization is restricted to the core part (Wu et al., 2004, 2007).

The Jiamiao area in the western part of the Luotian Dome was mapped as Paleoproterozoic metamorphic supracrustal suites named Dabie Group in a previous geological survey. Several granitic gneiss bodies and minor gneissic granites have been identified from the traditionally alleged Dabie Group in the present 1:50,000 mapping project, while Archean basements and supracrustal rocks from the original Dabie Group are mainly enclosed as fragments and lenses (Figure 2). The newly discovered granitic gneisses mainly consist of monzonitic gneisses and subordinate tonalitic gneisses, granodioritic gneisses, and syenitic gneisses with

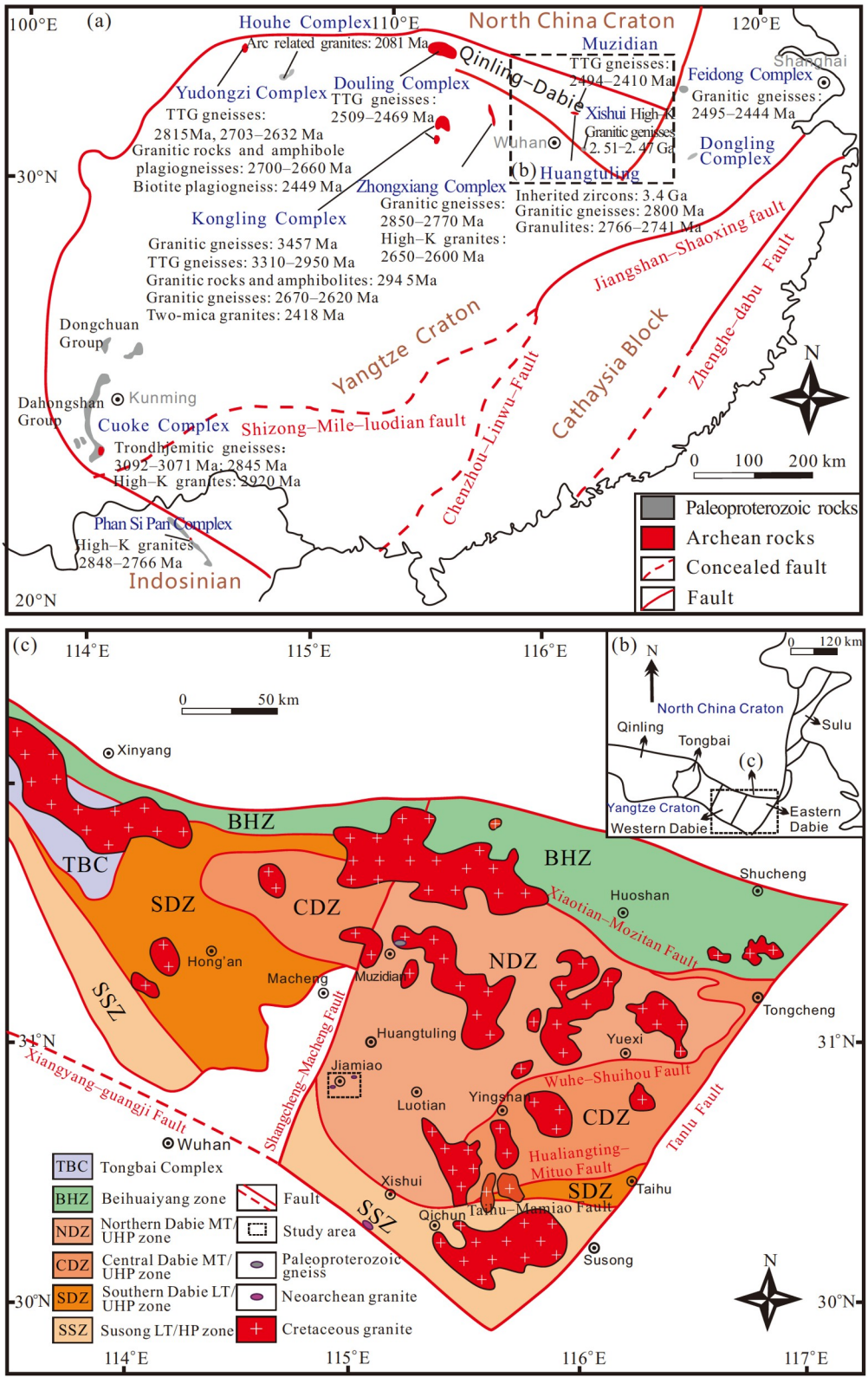

Figure 1 The Archean and Paleoproterozoic outcrops in the Yangtze Craton ((a), modified from Zhao et al., 2020); schematic geological map for Qinling-Dabie-Sulu orogenic belt (b) and sketch geological map of the Dabie orogen ((c), modified from Lei and Wu, 2008). Data source: Kongling Complex (Zheng et al., 2006; Jiao et al., 2009; Gao et al., 2011; Guo et al., 2014, 2015; Li et al., 2014; Qiu et al., 2019); Zhongxiang Complex (Wang et al., 2013; Zhou et al., 2015; Wang K et al., 2018; Wang Z et al., 2018; Huang et al., 2020); Cuoke Complex (Cui et al., 2020a, 2021); Phan Si Pan Complex(Zhao et al., 2019, 2020); Yudongzi Complex (Zhang et al., 2001; Hui et al., 2017; Zhou et al., 2018; Chen et al., 2019; Zhang S B et al., 2020); Houhe Complex(Wu et al., 2012); Douling Complex (Hu et al., 2013; Wu et al., 2014); Huangtuling granulite, gneiss (Wu et al., 2002, 2008; Xia et al., 2003; Sun et al., 2008); Muzidian gneiss (Qiu et al. 2021a); Xishui gneiss (Zhao et al., 2021); Feidong Complex (Tu et al., 2021).

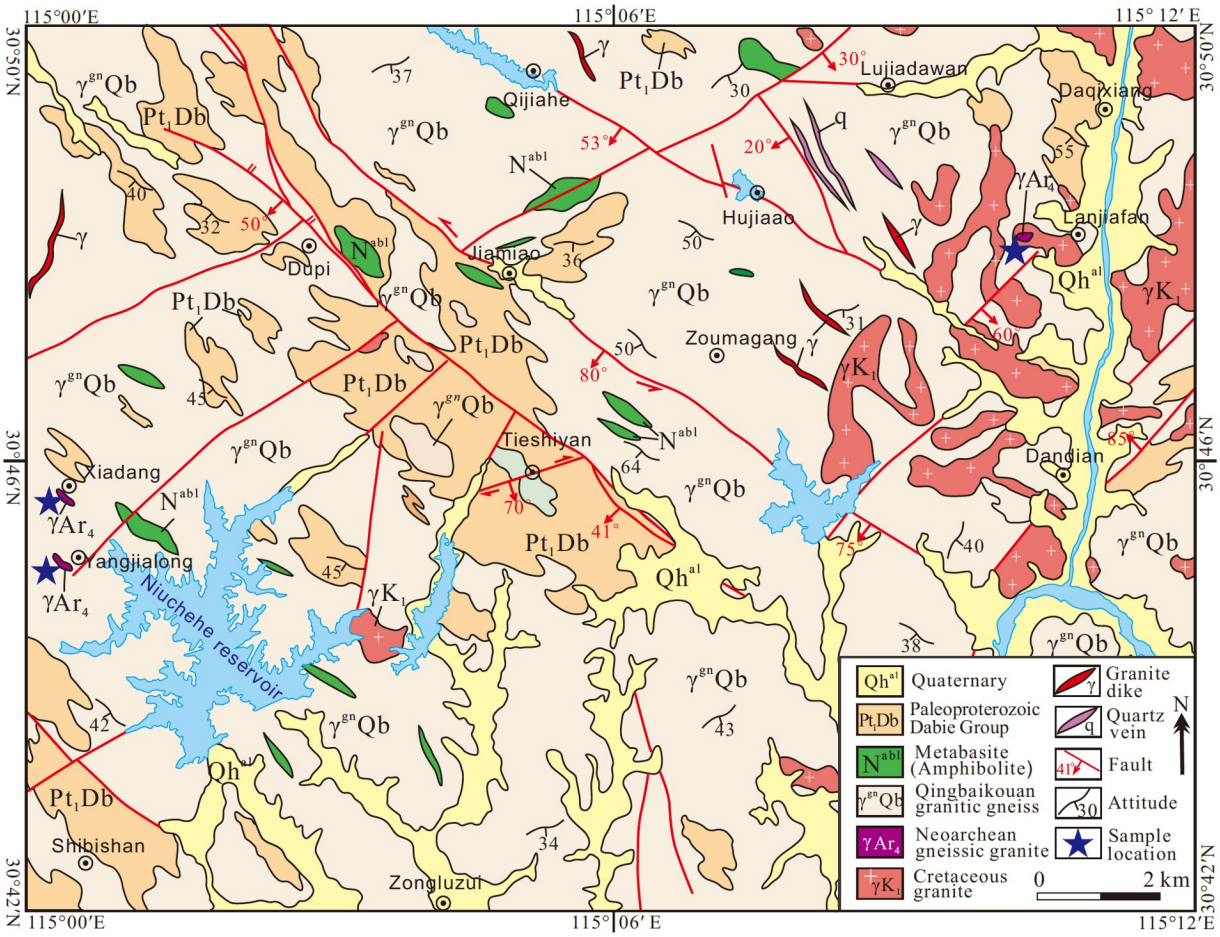

Figure 2 Simplified geological map of the Jiamiao area (based on our field survey) showing the sample locations.

protolith formed during Neoproterozoic (Wu et al., 2007). Melanocratic (mafic) enclaves are abundant. All of them exhibit features of ductile deformation and migmatization. Most of the granites, dendritically and planarly distributed in the east of the study area, are the Cretaceous porphyry syenogranite and monzogranite that were emplaced at ca. 130–120 Ma. Amphibolites are common and generally occur up to 1 km lenses in the study area. Two NW and NE trending faults are developed wherein the former cuts the latter one.

3. Sampling and methods

3.1 Sample description

The sampling locations and mineral assemblages of the three newly identified Neoarchean gneissic granite samples are shown in Table 1.

Sample XD-1G is a gneissic monzogranite, collected at highway S241, near Xiadang village, from a lens-shaped outcrop with a width of about 50 m (Figure 2). It is a grey-coloured weakly foliated rock with K-feldspar porphyroblasts and gneissic fabric. K-feldspar porphyroblasts (0.8×1.2–2×3 cm) constitute ~6% of the rock (Figure 3a). Epidotite and 1–10 cm long lenticular to sub-angular amphibolite enclaves are contained in these rocks. The groundmass mineral assemblage comprises K-feldspar (22%), plagioclase (43%), quartz (19%), biotite (13%), and hornblende (3%) (Figure 3b), suggesting it belongs to monzogranite. K-feldspar shows grid twinning and perthitic intergrowth, and contains inclusions of quartz, feldspar, and mica. Plagioclase laths show polysynthetic twinning and moderate sericitization and myrmekitic growth at contact with K-feldspar. Electron probe microanalyses confirm their oligoclase composition (Appendix Table S1, https://link.springer.com, Figure 4). Hornblende shows biotite corona due to alteration, while biotite shows chloritization at places. Accessory minerals include zircon, titanite, epidote and pyrite.

Sample LJF-2G, collected from the Lanjiafan quarry, is a grey, medium to fine grained gneissic syenogranite with amphibolite enclaves (Figure 2). It shows a more pronounced gneissosity than the previous outcrop and Cretaceous monzogranite intrusion nearby. The contact of the intrusion is marked by chilled margin and the development of a biotite-rich band in the host monzogranite (Figure 3c). The syeno-

Table 1 Sampling locations and mineral assemblages of Neoarchean gneissic granites in the Jiamiao area[a)]

Sample	Location	Coordinate	Lithology	Main minerals	Accessory minerals	Upper intercept ages (U-Pb)
XD-1G	Xiadang	115°0′28″N 30°45′42″E	Gneissic monzogranite	Kfs (27%), Pl (40%), Qtz (18%), Bt (12%), Hb (3%)	Zr, Py, Ttn, Ep	2645±30 Ma (MSWD=1.7)
LJF-2G	Lanjiafan	115°10′2″N 30°48′6″E	Gneissic syenogranite	Kfs (55%), Pl (12%), Qtz (24%), Bt (8%)	Zr, Ap, Ttn, Py, Mag, Aln	2630±37 Ma (MSWD=1.1)
YJL-5G	Yangjialong	115°0′26″N 30°45′2″E	Gneissic granodiorite	Pl (55%), Kfs (15%), Qtz (19%), Hb (10%), Bt (1%)	Ttn, Zr, Ap, Mag, Py, Aln	2497±29 Ma (MSWD=3.1)

a) Kfs, K-feldspar; Pl, plagioclase; Qtz, quartz; Hb, hornblende; Bt, biotite; Ep, epidote; Ttn, titanite; Zr, zircon; Ap, apatite; Mag, magnetite; Py, pyrite; Aln, allanite

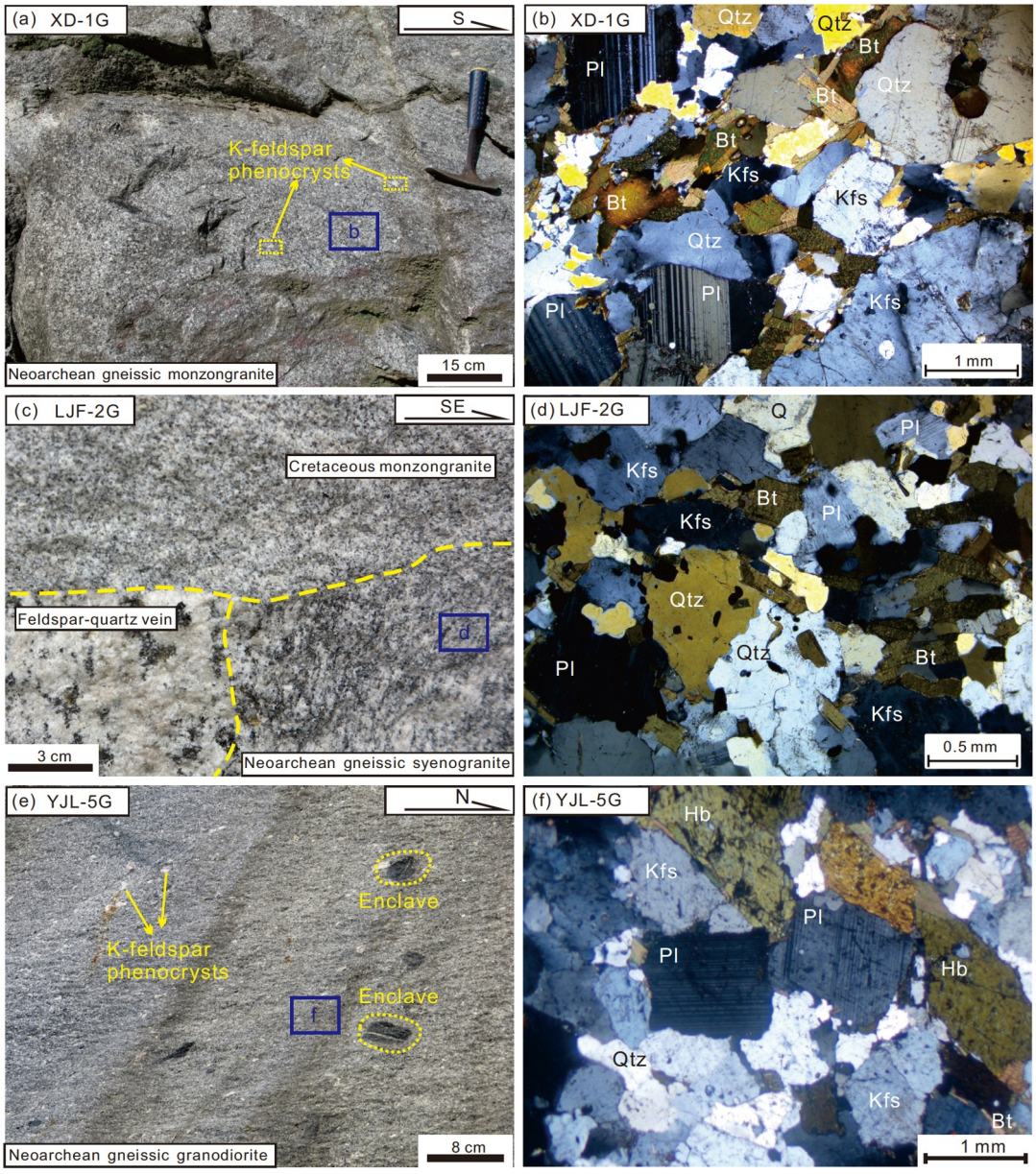

Figure 3 Outcrop photographs ((a), (c), (e)) and photomicrographs ((b), (d), (f)) of Neoarchean gneissic granite in the Jiamiao area. (a), (b) Xiadang monzonitic granite; (c) the contact relationship between Neoarchean syenogranite and Cretaceous granites in the Lanjiafan village; (d) photomicrograph for Lanjiafan Neoarchean syenogranite; (e), (f) Yangjialong Neoarchean granodiorite. Kfs, K-feldspar; Pl, plagioclase; Qtz, quartz; Hb, hornblende; Bt, biotite.

granite comprises K-feldspar (55%), plagioclase (12%), quartz (24%), and biotite (8%) (Figure 3d). K-feldspar shows Carlsbad twinning with inclusions of fine quartz, feldspar and mica. Plagioclase grains show typical polysynthetic twinning and have a small extinction angle, indicating sodic plagioclase composition, further supported by their oligoclase and andesine compositions in the An-Ab-Or diagram (Figure 4). Accessory minerals include zircon, titanite, apatite, allanite, magnetite, and pyrite.

Sample YJL-5G, collected from highway S241 near Yangjialong village, is a grey gneissic granodiorite, whose lensoid outcrop extends for about 80 m within Neoproterozoic granitoids (Figure 2). The rock shows porphyraceous texture, gneissic structure and have abundant lenticular to subrounded rock enclaves, which are generally 0.5×1–8×15 cm in size consisting of hornblendite and fine-grained amphibolite (Figure 3e). K-feldspar phenocrysts are pink, subhedral, 0.8×1.5–2×4 cm in size, and account for ~5% of the bulk, while fine-grained matrix consists of K-feldspar (10%), plagioclase (58%), quartz (20%), biotite (1%) and hornblende (11%) (Figure 3f). K-feldspar in the groundmass shows grid twinning, perthitic growth, and moderate kaolinization. Plagioclase shows minor sericitization, epidotization, well-preserved polysynthetic twinning, and a small extinction angle. They fall into the oligoclase composition field in the An-Ab-Or diagram (Figure 4). Hornblende shows slight epidotization, while biotite shows slight chloritization. The light isabelline to dark brownish-green colour of biotite suggests low-temperature formation. The accessory minerals include zircon, titanite, apatite, allanite, magnetite and pyrite.

3.2 Analytical methods

Zircon grains were separated using standard density and magnetic separation techniques after samples were crushed and washed, and were then handpicked under a binocular microscope, at the Yu-Neng Technology Service Limited Company for Rock & Mineral Separation, Langfang. Representative zircon grains and standard zircon samples (Penglai and Qinghu) were mounted on epoxy resin, and then polished to expose 1/3 to 1/2 crystal surface, at the State Key Laboratory of Isotopes, Guangzhou Institute of Geochemistry, Chinese Academy of Geological Sciences (SKLI, GIGCAS). Their morphology and internal structures were observed and documented with cathodoluminescence (CL), using a TescanMira3 instrument, at the Nanjing Hongchuang Geological Exploration Technology Service Co., LTD.

Inclusion and fracture free zircon grains were selected for *in-situ* zircon O isotope analysis (Figure 5), using a Cameca IMS-1280 SIMS at the SKLI, GIGCAS. The $^{133}Cs^{+}$ primary ion beam was accelerated at 10 kV with an intensity of 2 nA. The ion beam diameter was maintained at 20 μm. The mass fractionation was corrected using zircon standard Penglai,

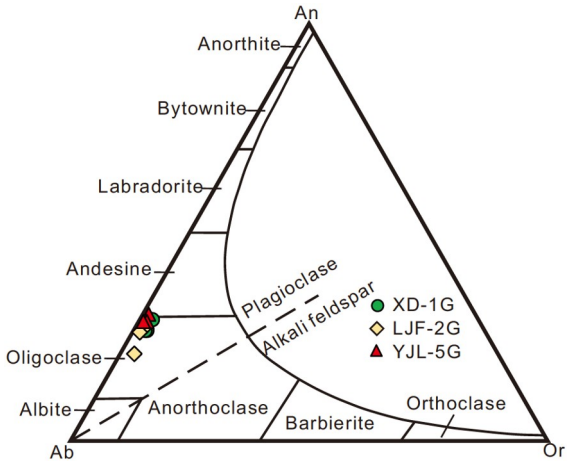

Figure 4 An-Ab-Or diagram for plagioclase of the Neoarchean gneissic granite in Jiamiao area.

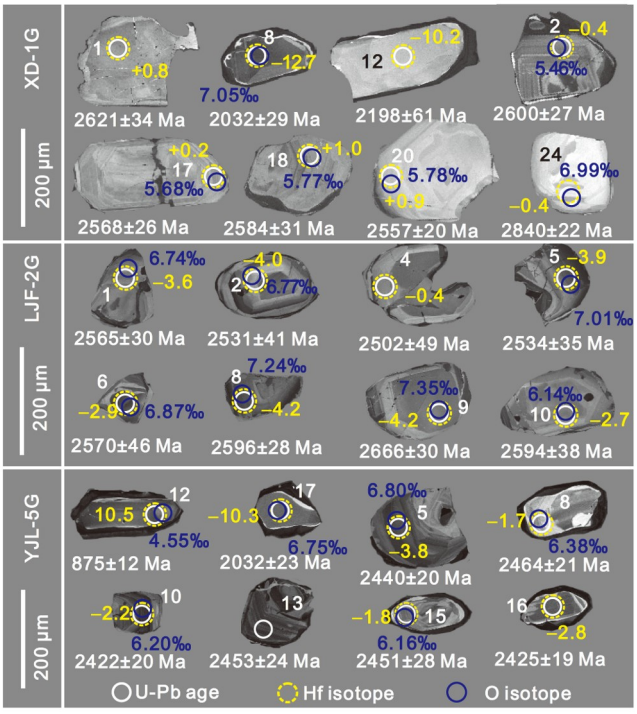

Figure 5 Representative cathodoluminescence images for zircon from the Jiamiao Neoarchean gneissic granites. Analytical spots as well the results of U-Pb-Hf-O data are also shown.

while zircon standard Qinghu was employed as an unknown sample for quality control. The analyses yielded a weighted mean $\delta^{18}O$ value of 5.31±0.10‰ (2SD) for the Qinghu zircons, which is consistent with the recommended value of 5.4 ±0.2‰ within analytical error (Li et al., 2013). For further details on the analytical procedure refer to Yang et al. (2018).

Zircon U-Pb isotopes and trace element abundances were simultaneously determined by LA-ICP-MS at Wuhan Sample Solution Analytical Technology Co., Ltd, using a COMPexPro 102 ArF excimer laser attached to an Agilent

7700e ICP-MS. The spot size and frequency of the laser were set at 32 μm and 6 Hz, respectively. Zircon standard 91500 and glass NIST610 were used as external standards for U-Pb dating and trace element calibration, respectively. Details on the operating conditions for the laser ablation system and the ICP-MS instrument, and data reduction are the same as described in Zong et al. (2017). Raw ICP-MS data were processed by ICPMSDataCal (Liu Y S et al., 2008) software, and the common lead correction was carried out by using the ComPbCorr#3_15G program (Andersen, 2002). Zircon U-Pb age concordia plots and weighted mean ages were obtained by using Isoplot/Ex_ver3 (Ludwig, 2003).

In situ zircon Lu-Hf isotopic ratios were analyzed using a Multiple Collector ICPMS (Thermo Fisher Scientific Neptune Plus) with a Coherent Geolas HD laser ablation system, at the Wuhan Sample Solution Analytical Technology Co., Ltd. The laser spot size was set at 44 μm and the frequency at 8 Hz. Detailed operating conditions are provided in Hu et al. (2012). Zircon standards 91500 and GJ-1 were used to ensure data quality, which gave external precision (2SD) better than 0.000020, consistent with recommended values within the error limits. Raw data were reduced off-line by the ICPMSDataCal program (Liu et al., 2010).

The whole rock major and trace elemental analyses were performed at the Central South Mineral Resources Supervision and Testing Center of the Ministry of Natural Resources. Fresh samples were crushed and pulverized to 200 mesh. Major element analyses were performed on fused glass disks using an X-ray fluorescence spectrometer (XRF) (Panalytical Axios Max). International standards GSR-01, GSR-02, GSR-03 and GSR-09 were utilized for analytical quality control. The precision of XRF analysis is better than 5%, and FeO was measured separately by titration.

Electron probe analysis of plagioclase laths was done at the Central South Mineral Resources Supervision and Testing Center of the Ministry of Natural Resources. The plagioclase laths were delineated under a polarizing microscope and then coated with carbon by employing a coating machine (KYKY SBC-2) to ensure good conductivity on the surface of the samples. The electron probe (Shimadzu EPMA-1600) was used to determine the major oxide concentrations. The operating conditions were set at 15 kV accelerating voltage, 10 nA probe current, and 5 μm beam diameter. The measured data were calibrated by atomic number correction (FZ), absorption correction (FA) and fluorescence correction (FF).

4. Results

4.1 Zircon U-Pb ages

Zircon grains from sample XD-1G are pale yellow, translucent, euhedral to subhedral, plate-columnar, and 100–400 μm in length with aspect ratios of 1–2.5, and commonly contain fine inclusions. Most analyzed zircons display bright luminescence with visible oscillatory zoning, indicating a magmatic origin, while a few zircon grains show dark margins and no visible oscillatory zoning of metamorphic origin (Figure 5). An analysis of metamorphic zircon (spot 12#) showed low Th/U ratio (0.09) and total REE content (98.1 ppm, 1 ppm=1 μg g^{-1}) and yielded a $^{207}Pb/^{206}Pb$ age of 2198±61 Ma (Table 2 and Appendix Table S2). Two other zircon grains (spots 8# and 21#) with younger $^{207}Pb/^{206}Pb$ ages of 2032±29 Ma and 1968±31 Ma were probably affected by recrystallization considering their dark luminescence and blurred oscillatory zoning (Figure 5), high Th/U ratios (0.73 and 0.79), and ΣREE (1320 and 1239 ppm) with REE patterns similar to magmatic zircon (Figure 6a) (Dong et al., 2017). A single old grain (spot 24#) with $^{207}Pb/^{206}Pb$ age of 2840±22 Ma exhibits oscillatory zoning (Figure 5) and a high Th/U ratio of 2.1, indicating a xenocrystic magmatic zircon. Three grains (spot 1#, 3# and 14#) have relatively high LREE contents (Figure 6a), most likely reflecting the presence of LREE-rich phosphate mineral inclusions (Figure 5). The remaining 17 analytical spots show high Th/U ratios (0.19–0.55), left-leaning chondrite normalized REE patterns, and positive Ce and negative Eu anomalies (Figure 6a), collectively indicating a magmatic origin. These 17 analyses define a discordia line with upper and lower intercept ages of 2645±30 and 638±140 Ma (MSWD=1.7), respectively. Since the studied zircons might have experienced variable lead loss, the upper intercept age of 2645±30 Ma possibly represents the crystallization age (Figure 7a).

Zircon grains from sample LJF-2G are pale yellow, translucent, euhedral to subhedral, and plate-columnar with some dotted or acicular inclusions. They are 80–200 μm in length with aspect ratios of 1–2. Most of them display gray luminescence with core-rim structure, noticeable oscillatory zoning, and dark and narrow overgrowth rims (Figure 5). Ten analyzed zircon grains show HREE enriched, left-inclined chondrite normalized REE patterns, and positive Ce and negative Eu anomalies (Figure 6b), with Th/U ratios of 0.59–1.35 (average 0.88), all indicating a magmatic origin. All the analyses define a discordia line with the upper and lower intercept ages of 2630±27 and 982±370 Ma (MSWD=1.13), respectively. Similarly, in view of lead loss, the upper intercept age of 2630±27 Ma possibly represents the crystallization age (Figure 7a).

Zircon grains from sample YJL-5G are pale yellow, transparent to translucent, euhedral to subhedral, and plate-columnar, with tiny inclusions. They are 80–250 μm long with aspect ratios of 1–3. Most of them show core-rim structure with dark and narrow rims, and two different types of core (Figure 5). The first type of zircon cores (spots 9# and 17#) show no or weak zoning and have low Th/U ratios (0.11 and 0.03) and low REE content (30.7 and 37.9 ppm, re-

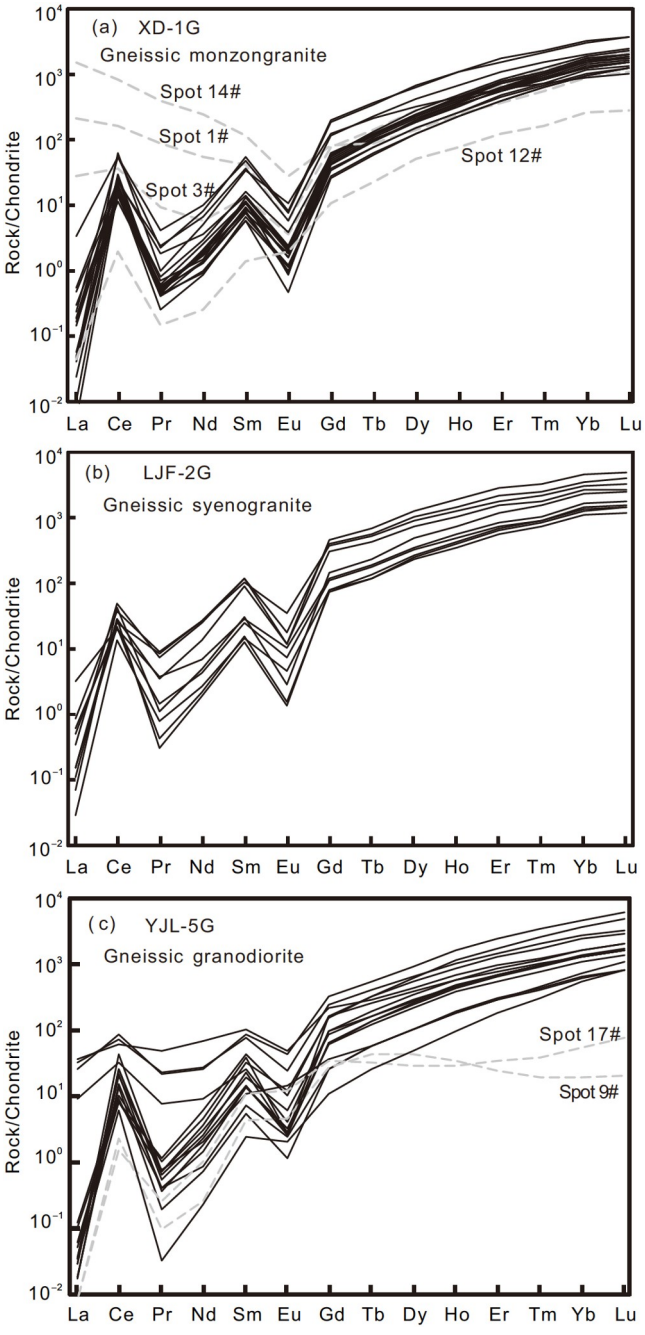

Figure 6 Chondrite normalized REE patterns for zircons from the Jiamiao Archean gneissic granite. Chondrite data from Sun and McDonough (1989).

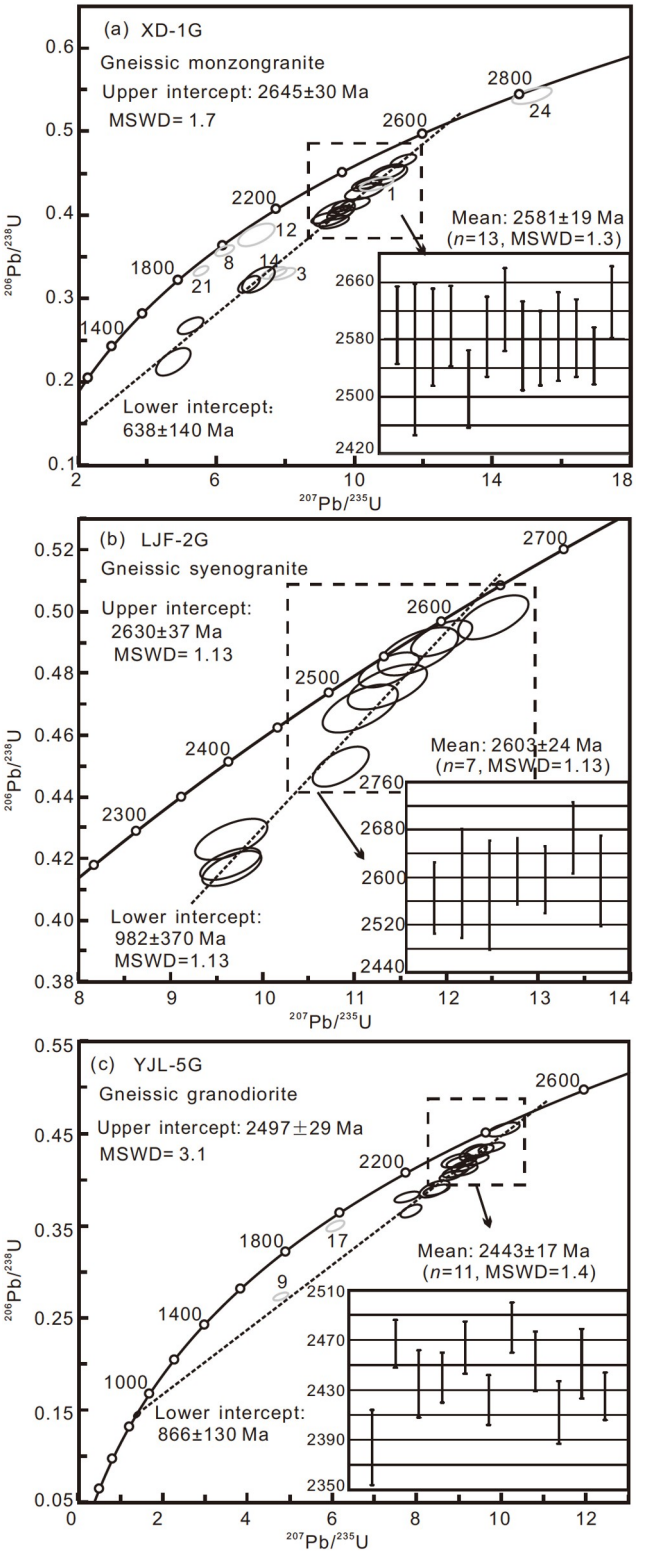

Figure 7 Concordia diagram of LA-ICP-MS zircon U-Pb data of the Jiamiao Archean gneissic granite (the grey cycles were excluded for the age calculation).

spectively), flat chondrite normalized HREE patterns, and absence of negative Eu anomaly (Figure 6c), indicating a metamorphic origin. Their $^{207}Pb/^{206}Pb$ ages are 2051±26 and 2032±23 Ma, respectively. Spot 12#, another analysis of type 1 core, with a $^{206}Pb/^{238}U$ age of 875±8 Ma, shows dark luminescence and a weakly planar structure. It has a relatively high Th/U ratio (0.83) and high REE content (1384 ppm) with a left-leaning REE pattern, suggesting it is a magmatic grain affected by recrystallization. The second type zircon cores show clear oscillatory zoning, high Th/U ratios (0.19–0.72), and HREE enriched REE patterns with positive Ce and negative Eu anomalies (Figure 6c), indicating a magmatic origin. These zircons plot along a discordia line with upper

Table 2 Zircon LA-ICP-MS U-Pb isotopic data for the Jiamiao Neoarchean granites[a)]

Spot	Th (ppm)	U (ppm)	Th/U	$^{207}Pb/^{206}Pb$		$^{207}Pb/^{235}U$		$^{206}Pb/^{238}U$		$^{207}Pb/^{206}Pb$		$^{206}Pb/^{238}U$		Concordia
				Ratios	1σ	Ratios	1σ	Ratios	1σ	Age (Ma)	1σ	Age (Ma)	1σ	
Gneissic monzogranite (XD-1G)														
2	218	458	0.48	0.1744	0.0030	9.998	0.1754	0.4132	0.0031	2600	27	2230	14	91%
4	62.4	180	0.35	0.1694	0.0052	9.391	0.2503	0.4020	0.0062	2552	53	2178	29	90%
5	82.7	211	0.39	0.1726	0.0038	10.26	0.2284	0.4280	0.0041	2583	34	2296	18	93%
6	118	432	0.27	0.1423	0.0046	5.242	0.1499	0.2672	0.0042	2255	58	1526	21	79%
7	116	295	0.39	0.1743	0.0031	10.936	0.2024	0.4515	0.0038	2599	28	2402	17	95%
9	96.3	269	0.36	0.1653	0.0030	9.105	0.1553	0.3964	0.0027	2511	27	2153	13	92%
10	104	259	0.40	0.1727	0.0032	9.400	0.1743	0.3915	0.0033	2584	28	2130	15	89%
11	85.9	217	0.40	0.1767	0.0035	10.98	0.2219	0.4474	0.0048	2622	29	2384	22	94%
13	99.7	214	0.47	0.1714	0.0031	10.33	0.1702	0.4373	0.0032	2571	31	2338	14	94%
15	79.8	415	0.19	0.1620	0.0053	7.203	0.1913	0.3225	0.0063	2476	57	1802	31	82%
16	139	533	0.26	0.1585	0.0035	6.930	0.1241	0.3171	0.0039	2440	38	1775	19	82%
17	114	291	0.39	0.1711	0.0026	9.557	0.1323	0.4052	0.0024	2568	26	2193	11	91%
18	76.4	238	0.32	0.1727	0.0031	9.574	0.1579	0.4021	0.0030	2584	31	2179	14	90%
19	120	280	0.43	0.1725	0.0028	10.41	0.1534	0.4375	0.0027	2582	27	2339	12	94%
20	80.0	213	0.37	0.1699	0.0024	9.649	0.1308	0.4110	0.0028	2557	20	2219	13	92%
22	258	821	0.31	0.1532	0.0080	4.730	0.2038	0.2239	0.0067	2382	91	1303	35	68%
23	205	376	0.55	0.1778	0.0027	11.395	0.1548	0.4649	0.0029	2632	25	2461	13	96%
8	558	761	0.73	0.1252	0.0021	6.225	0.1070	0.3572	0.0025	2032	29	1969	12	98%
12	11.5	129	0.09	0.1376	0.0047	7.139	0.2188	0.3762	0.0057	2198	61	2059	27	96%
21	475	603	0.79	0.1208	0.0021	5.546	0.0870	0.3329	0.0022	1968	31	1853	11	96%
24	127	60.5	2.10	0.2017	0.0031	15.14	0.2329	0.5432	0.0042	2840	22	2797	18	99%
1	147	314	0.47	0.1765	0.0035	10.63	0.1947	0.4366	0.0034	2621	34	2335	15	93%
3	172	484	0.36	0.1728	0.0032	7.903	0.1542	0.3292	0.0029	2585	30	1834	14	80%
14	77.2	218	0.35	0.1677	0.0036	7.647	0.1462	0.3307	0.0031	2535	37	1842	15	82%
Gneissic syenogranite (LJF-2G)														
1	107	174	0.62	0.1708	0.0033	11.38	0.2170	0.4812	0.0038	2565	30	2533	16	99%
2	85.1	145	0.59	0.1673	0.0040	9.650	0.2147	0.4183	0.0034	2531	41	2253	15	92%
3	213	210	1.01	0.1733	0.0047	11.36	0.2841	0.4756	0.0048	2590	46	2508	21	97%
4	99.9	131	0.76	0.1645	0.0047	9.664	0.2587	0.4262	0.0044	2502	49	2289	20	94%
5	169	282	0.60	0.1676	0.0037	9.668	0.2126	0.4168	0.0037	2534	35	2246	17	93%
6	736	688	1.07	0.1712	0.0046	11.06	0.2728	0.4686	0.0052	2570	46	2478	23	97%
7	382	291	1.31	0.1754	0.0032	11.95	0.2202	0.4913	0.0039	2610	28	2576	17	99%
8	434	564	0.77	0.1740	0.0030	10.85	0.2036	0.4497	0.0043	2596	28	2394	19	95%
9	175	130	1.35	0.1814	0.0037	12.51	0.2545	0.4983	0.0047	2666	30	2606	20	98%
10	61.2	85.2	0.72	0.1738	0.0044	11.69	0.2889	0.4871	0.0052	2594	38	2558	22	99%
Gneissic granodiorite (YJL-5G)														
1	616	853	0.72	0.1534	0.0026	8.905	0.1394	0.4211	0.0030	2384	30	2265	13	96%
2	436	672	0.65	0.1563	0.0030	8.403	0.1421	0.3899	0.0036	2416	34	2122	17	92%
3	48.5	181	0.27	0.1611	0.0021	9.151	0.1142	0.4106	0.0023	2467	19	2217	10	94%
4	151	249	0.61	0.1580	0.0025	8.901	0.1269	0.4085	0.0026	2435	27	2208	12	94%
5	97.8	490	0.20	0.1585	0.0021	9.101	0.1185	0.4150	0.0024	2440	20	2238	11	95%
6	77.4	223	0.35	0.1475	0.0025	7.756	0.1212	0.3813	0.0026	2317	30	2082	12	94%
7	343	1389	0.25	0.1575	0.0023	8.455	0.1229	0.3885	0.0025	2428	23	2116	12	92%
8	106	276	0.38	0.1608	0.0021	9.370	0.1285	0.4214	0.0026	2464	21	2267	12	95%
10	174	517	0.34	0.1568	0.0019	9.322	0.1291	0.4299	0.0035	2422	20	2305	16	97%
11	151	309	0.49	0.1623	0.0021	9.760	0.1251	0.4350	0.0023	2480	20	2328	10	96%
12	218	264	0.83	0.0685	0.0013	1.376	0.0273	0.1454	0.0014	884	37	875	8	99%
13	189	445	0.42	0.1597	0.0024	10.04	0.1523	0.4546	0.0030	2453	24	2415	13	99%
14	51.9	95.4	0.54	0.1560	0.0024	9.042	0.1421	0.4194	0.0026	2412	25	2258	12	96%
15	131	258	0.51	0.1595	0.0026	9.466	0.1396	0.4304	0.0031	2451	28	2307	14	96%
16	152	472	0.32	0.1571	0.0019	8.797	0.1068	0.4050	0.0022	2425	19	2192	10	94%
18	50.1	267	0.19	0.1551	0.0019	7.840	0.1010	0.3659	0.0028	2403	18	2010	13	90%
9	14.1	126	0.11	0.1266	0.0020	4.780	0.0737	0.2734	0.0016	2051	26	1558	8	86%
17	5.40	159	0.03	0.1252	0.0017	6.062	0.0874	0.3501	0.0025	2032	23	1935	12	97%

a) The data in grey shaded are excluding in age calculation

and lower intercept ages of 2497±29 and 866±130 Ma (MSWD=3.1), respectively, and the upper intercept age therefore represents the crystallization age (Figure 7c).

4.2 Zircon Lu-Hf isotopes

In situ Hf isotope analysis was performed on the same domains as U-Pb dating and the results are presented in Table 3 and Figure 8. Generally, all zircons have $\varepsilon_{Hf}(t)$ values ranging from −4.2 to +3.7, corresponding to T_{DM2} ages of 3.35 to 3.00 Ga.

Thirteen Neoarchean magmatic zircon grains from gneissic monzogranite (XD-1G) have $^{176}Lu/^{177}Hf$ ratios of 0.000396–0.000834 with an average value of 0.000668. They have ε_{Hf} (2645 Ma) values from −0.9 to +3.7 (average=+0.5) and T_{DM2} ages from 3186 to 2909 Ma (average=3100 Ma) (Table 3). The xenocrystic zircon (spot 24#) has a ε_{Hf} (2840 Ma) value of −0.4 with a T_{DM2} age of 3308 Ma (Table 3) and the two recrystallized zircon grains (spot 8# and 21#) have higher $^{176}Lu/^{177}Hf$ ratios (0.001315 and 0.001192) than the Neoarchean magmatic zircons, assumably implying alteration by high $^{176}Lu/^{177}Hf$ fluids during the recrystallization. They have $\varepsilon_{Hf}(t)$ values of −12.7 and −12.6 with T_{DM2} ages of 3416 and 3362 Ma, respectively (Table 3). One metamorphic zircon grain (spot 12#) displays a lower $^{176}Lu/^{177}Hf$ ratio of 0.000245 and $^{176}Hf/^{177}Hf$ ratio of 0.281100, corresponding a ε_{Hf}(2198 Ma) value of −10.2 and a T_{DM2} age of 3396 Ma (Table 3).

Ten Neoarchean magmatic zircon grains from the gneissic

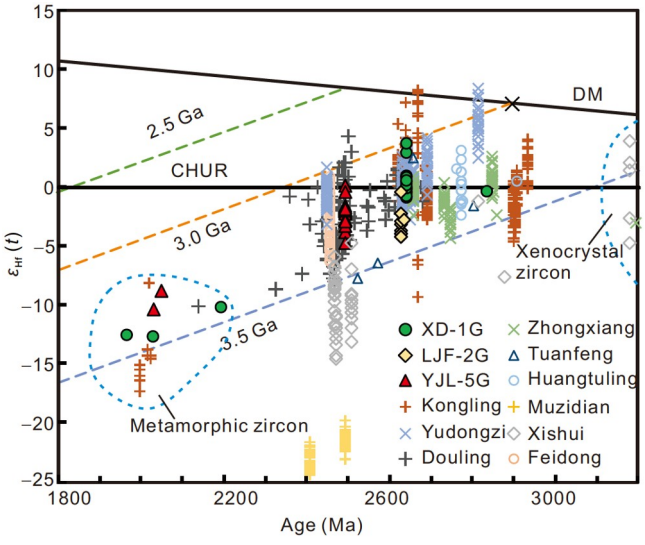

Figure 8 Compilation of zircon Hf isotopic data for rocks from the major Archean terranes (Yudongzi, Douling, Huangling, Zhongxiang, Huangtuling, Tuanfeng, Muzidian, Feidong, Jiaomiao) in the Yangtze Craton. Data source: Yudongzi (Hui et al., 2017; Zhou et al., 2018); Douling (Hu et al., 2013); Kongling (Chen et al., 2013); Zhongxiang (Wang Z et al., 2018, Zhou et al., 2015); Huangtuling (Lei and Wu, 2008); Tuanfeng (Qiu et al., 2020); Xishui (Zhao et al., 2021); Muzidian (Qiu et al., 2021a); Feidong (Tu et al., 2021). The quoted data were recalculated according to the Hf isotopic parameters mentioned in this paper.

syenogranite (LJF-2G) have $^{176}Lu/^{177}Hf$ ratios between 0.000423 and 0.001278 (average=0.000833), The $^{176}Hf/^{177}Hf$ ratios range from 0.281009 to 0.281103 (average=0.281046), with corresponding ε_{Hf}(2630 Ma) values of −4.2 to −0.4 (average=−3.1) and T_{DM2} ages from 3372 to 3141 Ma (average=3309 Ma) (Table 3).

Fourteen Neoarchean zircon grains from the gneissic granodiorite (YJL-5G) have $^{176}Lu/^{177}Hf$ ratios of 0.000349 to 0.002979 (average=0.000980), $^{176}Hf/^{177}Hf$ ratios of 0.281068 to 0.281326 (average=0.281166), ε_{Hf}(2497 Ma) values of −4.7 to +0.1 (average=−2.2), and T_{DM2} ages of 3297 to 3005 Ma (average=3145 Ma) (Table 3). The two Paleoproterozoic metamorphic zircon grains (spot 9# and 17#) have lower $^{176}Lu/^{177}Hf$ ratios of 0.000006 and 0.000025, higher $^{176}Hf/^{177}Hf$ ratios of 0.281228 and 0.281197, corresponding to $\varepsilon_{Hf}(t)$ values of −8.2 and −10.3 and T_{DM2} ages of 3192 and 3271 Ma, respectively (Table 3). The Neoproterozoic recrystallized zircon (spot 12#) has a high $^{176}Lu/^{177}Hf$ ratio of 0.002441 and $^{176}Hf/^{177}Hf$ ratio of 0.282572, corresponding to a $\varepsilon_{Hf}(t)$ value of +10.5 with a T_{DM2} age of 1069 Ma.

4.3 Zircon O-isotopes

Nine out of twelve analyses on magmatic domains from sample XD-1G have zircon $\delta^{18}O$ values ranging from 5.06 ±0.27‰ to 5.79±0.30‰ (average=5.59‰) (Figures 5 and 9), which show a positive linear correlation with their U-Pb ages (Appendix Figure S1). The decrease in primary zircon $\delta^{18}O$ values has mostly resulted from post-magmatic alteration (Appendix Figure S1) (Wan et al., 2015). The two metamorphic zircon grains (~2.0 Ga) have higher $\delta^{18}O$ values (7.05±0.21‰ and 6.81±0.18‰), while the xenocrystic zircon (~2.8 Ga) has a $\delta^{18}O$ value of 6.99±0.28‰ (Figure 9). Seven zircon grains from gneissic syenogranite sample LJF-2G yielded $\delta^{18}O$ values between 6.14±0.24‰ and 7.35 ±0.26‰ (average=6.87‰) (Figure 9). The lack of obviously linear correlation between zircon U-Pb ages and $\delta^{18}O$ values reveals the preservation of primary O isotope signatures in these zircons (Wan et al., 2015). Nine out of the eleven O isotope analyses from sample YJL-5G were targeted on magmatic domains, while the remaining two were done on metamorphic/recrystallized ones (Table 3, Figure 5). The magmatic zircons show $\delta^{18}O$ values from 5.95±0.17‰ to 7.09±0.17‰ (average=6.55‰). The absence of a clear correlation between the zircon $\delta^{18}O$ values and U-Pb ages suggests the zircon $\delta^{18}O$ values are primary (Appendix Figure S1) (Wan et al., 2015). The ~2.0 Ga metamorphic zircon has a $\delta^{18}O$ value of 6.75±0.22‰, similar to the magmatic zircon, while the Neoproterozoic recrystallized zircon has a lower $\delta^{18}O$ value of 4.55±0.22‰ (Figure 9).

Overall, the pristine Neoarchean magmatic zircon grains

Table 3 Hf-O isotopes for zircon from the Jiamiao Neoarchean gneissic granites[a)]

Spot	$^{176}Lu/^{177}Hf$	$^{176}Hf/^{177}Hf$	Age (Ma)	$(^{176}Hf/^{177}Hf)_i$	$\varepsilon_{Hf}(t)$	T_{DM} (Ma)	T_{DM2} (Ma)	$\delta^{18}O\pm2\sigma$ (‰)	Concordia
Gneissic monzogranite (XD-1G)									
2	0.000662	0.281104	2645	0.281072	−0.4	2962	3156	5.46±0.24	91%
4	0.000595	0.281193	2645	0.281164	2.9	2837	2955		90%
5	0.000659	0.281090	2645	0.281057	−0.9	2981	3186	5.42±0.32	93%
7	0.000734	0.281116	2645	0.281079	−0.1	2952	3139	5.73±0.23	95%
9	0.000396	0.281088	2645	0.281068	−0.5	2964	3161	5.65±0.19	92%
10	0.000737	0.281096	2645	0.281060	−0.8	2978	3180		89%
11	0.000703	0.281114	2645	0.281079	−0.1	2952	3139	5.06±0.27	94%
13	0.000714	0.281130	2645	0.281095	0.4	2931	3105		94%
17	0.000732	0.281125	2645	0.281089	0.2	2939	3118	5.68±0.21	91%
18	0.000667	0.281143	2645	0.281110	1.0	2910	3071	5.77±0.25	90%
19	0.000704	0.281220	2645	0.281186	3.7	2809	2909		94%
20	0.000550	0.281135	2645	0.281107	0.9	2913	3078	5.78±0.28	92%
23	0.000834	0.281139	2645	0.281098	0.5	2928	3099	5.79±0.30	96%
8	0.001315	0.281180	2032	0.281129	−12.7	2910	3416	7.05±0.21	98%
12	0.000245	0.281100	2198	0.281090	−10.2	2936	3396		96%
21	0.001192	0.281217	1968	0.281173	−12.6	2849	3362	6.81±0.18	96%
24	0.000386	0.280963	2840	0.280942	−0.4	3129	3308	6.99±0.28	99%
Gneissic syenogranite (LJF-2G)									
1	0.000586	0.281020	2630	0.280991	−3.6	3069	3338	6.74±0.17	99%
2	0.000758	0.281018	2630	0.280981	−4.0	3085	3360	6.77±0.18	92%
3	0.000975	0.281053	2630	0.281005	−3.1	3055	3309		97%
4	0.000423	0.281103	2630	0.281082	−0.4	2945	3141		94%
5	0.000555	0.281009	2630	0.280981	−3.9	3081	3358	7.01±0.26	93%
6	0.001249	0.281074	2630	0.281012	−2.9	3049	3293	6.87±0.21	97%
7	0.001270	0.281093	2630	0.281030	−2.2	3025	3255		99%
8	0.000713	0.281011	2630	0.280975	−4.2	3092	3372	7.24±0.19	95%
9	0.001278	0.281039	2630	0.280975	−4.2	3099	3372	7.35±0.26	98%
10	0.000529	0.281037	2630	0.281011	−2.7	3042	3289	6.14±0.24	99%
Gneissic granodiorite (YJL-5G)									
1	0.002979	0.281326	2497	0.281187	0.1	2833	3005	6.93±0.23	96%
2	0.002497	0.281242	2497	0.281125	−2.0	2915	3137	6.75±0.26	92%
3	0.000349	0.281154	2497	0.281138	−1.5	2872	3106		94%
4	0.000824	0.281173	2497	0.281134	−1.7	2882	3114		94%
5	0.000628	0.281102	2497	0.281073	−3.8	2962	3246	6.80±0.15	95%
6	0.000408	0.281068	2497	0.281049	−4.7	2991	3297	7.09±0.17	94%
7	0.001371	0.281154	2497	0.281090	−3.2	2949	3210		92%
8	0.000625	0.281163	2497	0.281133	−1.7	2881	3115	6.38±0.17	95%
10	0.000730	0.281152	2497	0.281118	−2.2	2904	3150	6.20±0.21	97%
11	0.000813	0.281142	2497	0.281104	−2.7	2923	3179	5.95±0.17	96%
14	0.000721	0.281162	2497	0.281128	−1.9	2889	3128	6.69±0.20	96%
15	0.000737	0.281165	2497	0.281130	−1.8	2886	3122	6.16±0.23	96%
16	0.000670	0.281133	2497	0.281102	−2.8	2924	3184		94%
18	0.000367	0.281189	2497	0.281171	−0.3	2827	3033		90%
12	0.002441	0.282572	875	0.282531	10.5	1001	1069	4.55±0.22	99%
9	0.000006	0.281228	2051	0.281227	−8.7	2749	3192		86%
17	0.000025	0.281197	2032	0.281196	−10.3	2791	3271	6.75±0.22	97%

a) The following parameters were used during the calculation: $\lambda^{176}Lu=1.867\times10^{-11}$ (Söderlund et al., 2004); $^{176}Lu/^{177}Hf_{Crust}=0.015$ (Griffin et al., 2002); $^{176}Hf/^{177}Hf_{CHUR}=0.282793$, $^{176}Lu/^{177}Hf_{CHUR}=0.0338$ (Iizuka et al., 2015), $^{176}Hf/^{177}Hf_{DM}=0.28325$, $^{176}Lu/^{177}Hf_{DM}=0.0384$ (Blichert-Toft and Albarède, 1997).

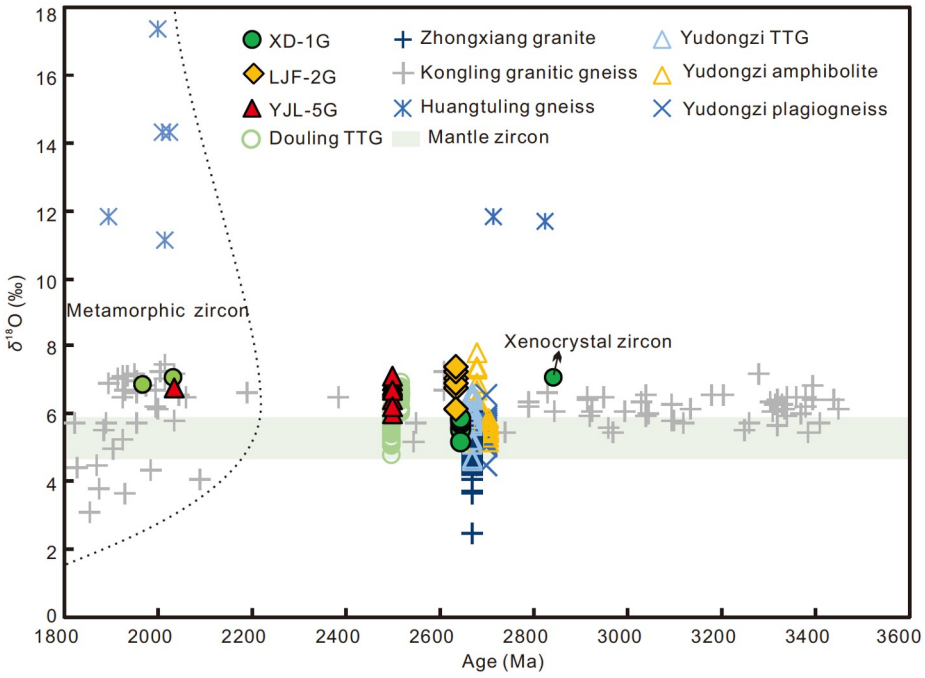

Figure 9 Compilation of zircon $\delta^{18}O$ data for rocks from the major Neoarchean-Paleoproterozoic terranes (Kongling, Yudongzi, Douling, Huangling, Zhongxiang, Jiamiao) in the Yangtze Craton. Data source: Yudongzi (Zhang S B et al., 2020); Douling (Wu et al., 2014); Kongling (Guo et al., 2014); Zhongxiang (Zhang S B et al., 2020); Huangtuling (Xia et al., 2003).

from the Jiamiao region have $\delta^{18}O$ values higher than the normal mantle zircon (5.3±0.6‰) (Valley et al., 1998). These $\delta^{18}O$ values are similar to those of Archean-Paleoproterozoic zircon from the Kongling, Zhongxiang, Yudongzi, and Douling complexes, but significantly lower than those of magmatic zircon from the Huangtuling gneiss (Figure 9). The ~2.0 Ga metamorphic zircon crystals from the Jiamiao rocks have $\delta^{18}O$ values consistent with the zircon from the Kongling granitic gneiss, but lower than those from the Huangtuling gneiss (Figure 9).

4.4 Whole-rock major elements

The whole-rock major element analyses of Jiamiao Neoarchean granites are presented in the Appendix Table S3. Five monzogranite (XD-1G-1h–5h) and three syenogranite (LJF-2G-1h–3h) samples have high SiO_2 (67.1–70.0 wt.%; 70.9–71.8 wt.%) and K_2O (3.34–4.53 wt.%; 4.09–4.24 wt.%) contents, and K_2O/Na_2O ratios (1.11–1.89; 1.21–1.41), but low Na_2O (2.40–3.00 wt.%, 2.96–3.38 wt.%) and CaO contents (1.61–2.64 wt.%; 1.53–1.81 wt.%), resembling high-K granites (Appendix Figure S2) (Zhang and Zhai, 2012; Laurent et al., 2014). On the contrary, three granodiorite (YJL-5G-1h–3h) samples have relatively low SiO_2 (64.8–66.0 wt.%) and K_2O (2.54–2.96 wt.%) contents and K_2O/Na_2O ratios (0.64–0.77), but high Na_2O (3.86–3.99 wt.%) and CaO (3.75–4.06 wt.%) contents, similar to geochemical characteristics of typical TTG (Appendix Figure S2).

5. Discussion

5.1 Neoarchean basement in the northeastern Yangtze Craton

The Kongling Complex represents the largest basement outcrop in the Yangtze Craton, and holds plentiful information in deciphering the evolution history of the early continental crust in the Yangtze Craton (Qiu et al., 2000; Zhang and Zheng, 2007; Jiao et al., 2009; Gao et al., 2011; Guo et al., 2015). Circa 3.8 Ga detrital zircons from sandstone samples of the Liantuo Formation in the Kongling area record the oldest geological archive for the Yangtze Craton (Zhang et al., 2006b). Besides, the Archean-Paleoproterozoic basement rocks are sporadically exposed in the Zhongxiang (Zhou et al., 2015; Wang Z et al., 2018; Huang et al., 2020), Yudongzi (Hui et al., 2017; Chen et al., 2019), Xishui (Zhao et al., 2021), Fiedong (Tu et al., 2021), Cuoke (Zhao et al., 2020; Cui et al., 2020a) and Phan Si Pan (Wang et al., 2016; Zhao et al., 2019) locations in the Yangtze Craton (Figure 1a). The presence of Archean basement in the northeastern Yangtze Craton, e.g., in the Dabie orogen, is of vital significance for the understanding of early crustal evolution of the Yangtze Craton, however, these are poorly explored. By far, Archean rocks are occasionally reported from the Dabie orogen. Three inherited zircon grains from the Muzidian granitic gneiss in the northern Dabie orogen have U-Pb ages of ~4.0 Ga (Qiu et al., 2021b), while the Huangtuling pelitic granulite contains 3.4, 2.95–2.90 and

~2.77 Ga inherited zircons (Wu et al., 2002; Lei and Wu, 2008; Sun et al., 2008). Meosoarchean-Neoarchean protolith ages are reported for Tuanfeng migmatite (Qiu et al., 2020) and Xishui gneiss (Zhao et al., 2021). It is obvious that these Archean zircons reported from the Dabie orogen were mainly inherited from either sedimentary sources or protolith of metamorphic rocks, whereas Archean rocks are rarely confirmed in this orogen yet. In this study we report the first occurrence of Archean rocks as a <100 m long lensoid gneissic granite outcrop in the Jiamiao area of the northern Dabie orogen. The Xiadang monzogranite (XD-1G) and Yangjialong granodiorite (YJL-5G), intruded by Neoproterozoic granites, contain several mafic enclaves (Figure 3a and 3e). These rocks show porphyroblastic texture with K-feldspar phenocrysts and granular grains in the groundmass (Figure 3b and 3f). They were emplaced at 2645±30 and 2497±29 Ma, respectively, and experienced metamorphism at ~2.0 Ga. The Lanjiafan syenogranite (LJF-2G) with medium-to-fine granular texture were emplaced at 2630±37 Ma and were intruded by Cretaceous granites (Figure 3c and 3d). These gneissic granites, in spite of limited exposure, provide direct and unambiguous evidence for the existence of Archean basement in the Dabie orogen, northeastern Yangtze Craton.

5.2 Archean crust formation and evolution: A unified basement in the Yangtze Craton?

Geochronologic data available in recent years have indicated the widespread occurrence of Archean-Paleoproterozoic crystalline basement in the Yangtze Craton. Whether these basements blocks were unified or represent separate microcontinents, continues to be a hotly debated issue (e.g., Zheng et al., 2006; Wu et al., 2012; Li et al., 2021; Zhao et al., 2021; Tu et al., 2021). The similar U-Pb ages and Hf isotopic characteristics of Archaean xenocrystic zircons from different lamproite diatremes suggest the existence of unexposed unified basement in the Yangtze Craton (Zheng et al., 2006)**.** It has been also suggested the Yangtze Craton is a unified terrane with the Kongling Complex as the continental core that grew to its present size through lateral and vertical accretion (Gao et al., 2011; Zhang and Zheng, 2013). In contrast, it is suggested that Yangtze Craton contain separated western and eastern parts that collided at ~2.0 Ga, considering the existence of 2.4–2.05 Ga magmatic zircons only in the western Yangtze Craton (Wu et al., 2012). Furthermore, the Yangtze Craton is thought to consist of the southern and northern blocks, based on the distinct pre-Neoproterozoic lithological assemblages and evolution histories (Li et al., 2021). On the other hand, some researchers focused on the petrological and geochemical features and proposed that the Yangtze Craton is constituted by several independent micro-nuclei during Paleoproterozoic (Cawood et al., 2020; Zhao et al., 2020, 2021).

The slightly depleted Hf isotopic compositions ($\varepsilon_{Hf}(t)$ values of −0.9 to +3.7, T_{DM2} ages of 3186 to 2909 Ma) and $\delta^{18}O$ values (average=5.59‰) of the zircon from the ~2.65 Ga gneissic monzogranite (XD-1G) discovered in this study suggest that the granites were generated by reworking of Mesoarchean crustal material with minor addition of juvenile crust. On the contrary, the zircon from the ~2.63 Ga (LJF-2G) syenogranite and ~2.50 Ga (YJL-5G) granodiorite have enriched Hf isotopic compositions (average $\varepsilon_{Hf}(t)$ values of −3.1 and −2.2, corresponding to T_{DM2} ages of 3309 and 3145 Ma) and high average $\delta^{18}O$ values of 6.87‰ and 6.55‰, indicating their possible derivation through the reworking of Paleo-Mesoarchean basement rocks with minor addition of supracrustal material. Considering the same emplacement age of monzogranite (XD-1G, ~2.65 Ga) and granodiorite (LJF-2G, ~2.63 Ga), the Neoarchean magmatic events in the northern Dabie orogen of the Yangtze Craton are characterized by reworking of Paleo-Mesoarchean crustal rocks, while the high zircon $\delta^{18}O$ values imply that supracrustal material may have already been recycled into their magma sources.

Despite the effects of crustal assimilation and source heterogeneity, zircon Hf isotopic compositions could provide important information on the nature of their host protoliths and the constraints on crustal growth. As mentioned above, zircon T_{DM2} ages (3.37–2.91 Ga, with a peak at 3.15 Ga) of the Jiaomiao Neoarchean granites indicate a crustal growth event during the Paleo- to Mesoarchean. Moreover, crustal growth as early as ~4.0 Ga is deduced by inherited zircons from the Muzidian gneiss in the northern Dabie orogen (Qiu et al., 2021a) (Figure 10). On the other hand, based on zircon Hf model ages (T_{DM2}), multiple stages of crustal growth have been interpreted for the Kongling Complex at 3.8–3.5, 3.3–3.2, 3.0–2.9 and 2.7 Ga (Gao et al., 2011; Chen et al., 2013; Zhang and Zheng, 2013; Li et al., 2018; Wei et al., 2019, 2020), the Zhongxiang Complex at 3.4–3.1 Ga (Wang K et al., 2018; Wang Z et al.,2018), the Phan Si Pan Complex at 3.9–3.8, 3.6, 3.3, 3.0–2.9 and 2.6–2.5 Ga (Zhao et al., 2019), the Cuoke Complex at 3.6, 3.5–3.4 and 3.1–2.9 Ga (Cui et al., 2020a, 2020b, 2021), the Yudongzi Complex at 3.4–2.6 Ga (Hui et al., 2017; Zhou et al., 2018; Chen et al., 2019; Zhang S B et al., 2020), the Douling Complex at 3.5–2.6 Ga (Hu et al., 2013; Wu et al., 2014) and the Xishui high-K gneiss at 3.8–3.7 and 3.5–3.4 Ga (Zhao et al., 2021). In addition, T_{DM2} ages of ~3.67 Ga inherited zircons from Neoproterozoic gneisses in the Yangkou outcrop from the Sulu orogen imply crustal growth during 4.17–3.90 Ga, with a peak at ~4.03 Ga (Zhou et al., 2020). Obviously, the present data underline different continental crustal evolution patterns recorded by several Archean-Paleoproterozoic complexes in the present-day nuclei of the Yangtze Craton (Figure 10).

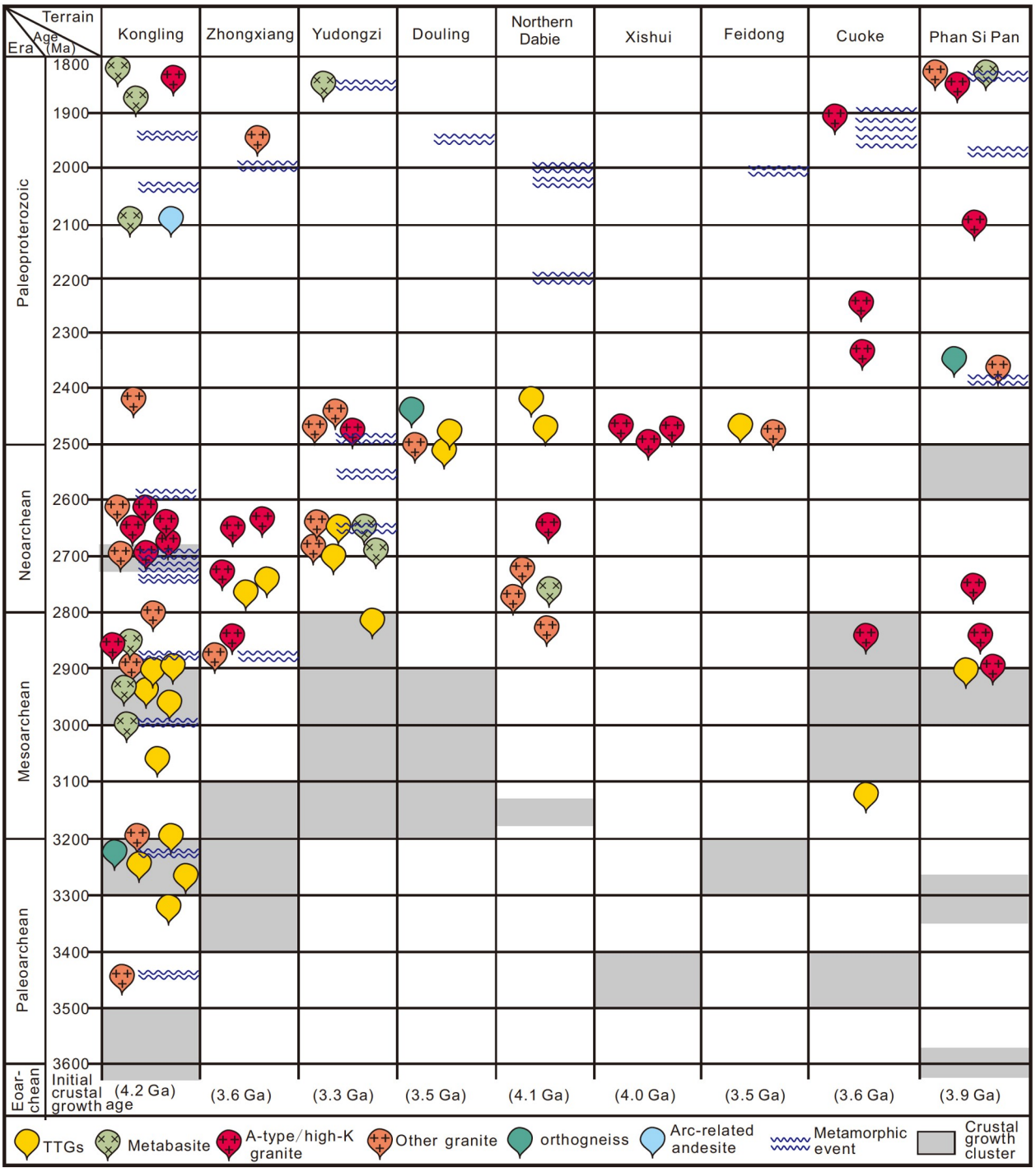

Figure 10 Major magmatic, metamorphic, and crustal growth and reworking events in different terranes of the Yangtze Craton during Archean to Paleoproterozoic. Data source: Kongling Complex (Jiao et al., 2009; Gao et al., 2011; Chen et al., 2013; Guo et al., 2014, 2015; Li et al., 2014; Qiu et al., 2019; Wei et al., 2019, 2020); Zhongxiang Complex (Wang et al., 2013; Zhou et al., 2015; Wang K et al., 2018; Wang Z et al., 2018; Huang et al., 2020); Cuoke Complex (Cui et al., 2020a, 2021); Phan Si Pan Complex (Nam et al., 2003; Zhao et al., 2019, 2020); Yudongzi Complex (Zhang et al., 2001, Zhang S B et al., 2020; Hui et al., 2017; Zhou et al., 2018; Chen et al., 2019); Douling Complex (Hu et al., 2013; Wu et al., 2014); Northern Dabie orogen including the Huangtuling, Muzidian, Tuanfeng and Jiamiao areas (Wu et al., 2002, 2008; Xia et al., 2003; Sun et al., 2008; Qiu et al., 2020, 2021a; This study); Xishui gneiss(Zhao et al., 2021); Feidong Complex (Tu et al., 2021).

Archean TTG rocks are rich in sodium and display high Na_2O/K_2O ratio (>1), which is mostly between 0.5 and 1 in high-K granites (Zhang and Zhai, 2012). The transition from Na-rich TTG rocks to high-K granite has been considered as one of the important signs on the stabilization of the cratonic lithosphere. Sporadic Archean-Paleoproterozoic basement exposures also record the transition in the Yangtze Craton, however, the timings of the transformation are not syn-

chronous (Figure 10). The transition was suggested to occur at ~2.92–2.77 Ga for the Phan Si Pan and Cuoke terrains in the southwest (Zhao et al., 2019), at ~2.88 and ~2.85 Ga for the Kongling and Zhongxiang complexes in the north (Wang Z et al., 2018; Wei et al., 2019), and at ~2.5 Ga for the Yudongzi Complex in the northwest (Hui et al., 2017; Zhou et al., 2018; Chen et al., 2019). The ~2.65–2.63 Jiamiao monzogranite (~2.65 Ga) and grandiorite (~2.63 Ga) have relatively high average K_2O (3.81% and 4.16%) and low Na_2O (2.79% and 3.11%) contents and thus high K_2O/Na_2O ratios (1.39 and 1.34) (Appendix Table S3 and Figure S1), suggesting that the presence of high K-granites in the northeastern Yangtze Craton could be as early as ~2.65 Ga, similar to the Archean basement in the eastern Jiaodong area of the North China (Yao et al., 2020). It can be concluded that the transition from Na-rich TTG to high-K granite, as well as the stabilization of lithosphere, was asynchronous amongst the different complexes/terranes of the Yangtze Craton. On the other hand, the ~2.5 Ga granodiorite (YJL-5G) as well as the 2.5–2.4 Ga Muzidian gneiss (Qiu et al., 2021a) show signatures similar to Na-rich TTG rocks, whereas the ~2.50 Ga protoliths of the Xishui gneisses in adjacent area are strongly peraluminous high-K granites. This observation implies a gradual transition from Na-rich TTG to the high-K granites in the Dabie orogen in the northeastern Yangtze Craton.

Besides, distinct tectono-thermal events during the Archean-early Paleoproterozoic are recorded by the different complexes/terrains within the Yangtze Craton. For instance, the Kongling Complex has experienced Mesoarchean-Neoarchean metamorphism at 3.00–2.94 and 2.75–2.70 Ga prior to ~2.0 Ga orogenic event (Qiu et al., 2000; Jiao et al., 2009; Guo et al., 2015; Wei et al., 2019). The Zhongxiang Complex records a metamorphic event at ~2.87 Ga, assumed to be related to an arc-continent collision event (Wang Z et al., 2018). The high grade metamorphic events at 2.65–2.49 Ga (Chen et al., 2019) and ~2.36 Ga (Nam et al., 2003) are reported for the Yudongzi and Phan Si Pan complexes, respectively. In the present case, the Jiamiao monzogranite (XD-1G) recorded ~2.2 Ga metamorphism (Figure 10). In short, all the exposed Archean complexes/terrains within the Yangtze Craton have experienced distinct patterns of crustal evolution and tectono-thermal process before 2.0 Ga, indicating that they may be individual microcontinents instead of a unified craton.

In spite of the distinct evolution process mentioned above, there is a joint metamorphic event at ~2.0 Ga recorded in these Archean-early Paleoproterozoic complexes/terrains within the Yangtze Craton (Zhang et al., 2006a; Yin et al., 2013; Li et al., 2014; Wang et al., 2016; Hui et al., 2017; Wang Z et al., 2018; Liu et al., 2019; Zhao et al., 2019; Cui et al., 2020a) (Figure 10). The Jiamiao Neoarchean granites also document metamorphism at ~2.0 Ga, which is synchronous with those recorded in the Muzidian gneiss, the Tuanfeng migmatite, and the Huangtuling granulite in the Dabie orogen (Wu et al., 2008; Qiu et al., 2020, 2021a). Collectively, this metamorphism may record the final collision/amalgamation of the above-mentioned individual microcontinents in building the Yangtze Craton, as syncollision magmatism, represented by the Zhongxiang 1.96–1.93 Ga granite (Wang et al., 2015) and the Tongbai ~1.96 Ga basic rocks (Zhang Q Q et al., 2020). A series of subduction-related rocks, including the 2.05–2.03 Ga Nb-rich mafic rocks (Han et al., 2018; Han and Peng, 2020), the Houhe ~2.08 Ga granitic rocks (Wu et al., 2012), and the Kongling ~2.15 Ga ophiolitic mélange (Han et al., 2017b; Zhou et al., 2021), mark the subduction among microcontinents just before the amalgamation of the Yangtze Craton. This observation suggests that the individual microcontinents collided to form the unified Yangtze Craton through subduction and collision at ~2.0 Ga, coinciding with the timing of the assembly of the Columbia supercontinent. Nevertheless, there is no Archean basement known from the southern Yangtze Craton by far and the widespread Meso-Neoproterozoic magmatic rocks were generally sourced from the Paleoproterozoic basement (Li et al., 2021), which hinders the understanding of the continental components in the southern Yangtze Craton and their involvement in building the unified craton at ~2.0 Ga, which thus needs further investigation.

6. Conclusions

(1) Three Neoarchean granitoids were emplaced in the Dabie orogen at 2645±30 (high-K monzogranite), 2630±37 (high-K syenogranite), and 2497±29 Ma (Na-rich granodiorite). They confirm the existence of a ~2.7–2.5 Ga crystalline basement in the northern Dabie orogen of the Yangtze Craton and provide important information for the early crustal evolution.

(2) Weakly enriched to depleted Hf isotopic compositions and high $\delta^{18}O$ values of zircons from the Jiamiao Neoarchean granites indicate that these rocks were mainly generated through the reworking of Paleo-Mesoarchean basement rocks with a minor contribution of supracrustal material.

(3) The Yangtze Craton may contain individual microcontinents that evolved separately before the ~2.0 Ga metamorphism, presumably leading to form a unified craton and synchronous with the assembly of the Columbia supercontinent. However, the lack of relevant data from the southeastern Yangtze Craton may abate such a conclusion, which should be solved in the future.

Acknowledgements *We would like to thank all the team members of the "1: 50,000 Regional Geological Survey in Macheng-Tuanfeng Area,*

Hubei Province" project for their help in field investigation and sample collection; Jing TAN, Xin SHAO, Guimei LU and Qing WANG for sample analyses and data processing. Profs. Hanwen ZHOU and Yunxu WEI are thanked for their thoughtful and constructive comments and suggestions on an earlier version of the manuscript. Three anonymous reviewers are thanked for their constructive comments and suggestions. Prof. Manoj PANDIT is also thanked for the linguistic polishing. This work was supported by the National Natural Science Foundation of China (Grant No. 41972242), the Regional Geological Survey Project of China Geological Survey (Grant Nos. DD20190050 & DD20221634), and the Open Fund of the Research Center for Petrogenesis and Mineralization of Granitoid Rocks (Grant Nos. PMGR202002 & PMGR202112).

References

Andersen T. 2002. Correction of common lead in U-Pb analyses that do not report ^{204}Pb. Chem Geol, 192: 59–79

Blichert-Toft J, Albarède F. 1997. The Lu-Hf isotope geochemistry of chondrites and the evolution of the mantle-crust system. Earth Planet Sci Lett, 148: 243–258

Cawood P A, Wang W, Zhao T, Xu Y, Mulder J A, Pisarevsky S A, Zhang L, Gan C, He H, Liu H, Qi L, Wang Y, Yao J, Zhao G, Zhou M F, Zi J W. 2020. Deconstructing South China and consequences for reconstructing Nuna and Rodinia. Earth-Sci Rev, 204: 103169

Chen K, Gao S, Wu Y, Guo J, Hu Z, Liu Y, Zong K, Liang Z, Geng X. 2013. 2.6–2.7 Ga crustal growth in Yangtze craton, South China. Precambrian Res, 224: 472–490

Chen Q, Sun M, Zhao G C, Zhao J H, Zhu W L, Long X P, Wang J. 2019. Episodic crustal growth and reworking of the Yudongzi terrane, South China: Constraints from the Archean TTGs and potassic granites and Paleoproterozoic amphibolites. Lithos, 326-327: 1–18

Cui X Z, Ren G M, Sun Z M, Wang P, Liu SL, Deng Q, Ren F, Pang W H. 2020a. Multiple tectonothermal events recorded in the Early Precambrian Cuoke Complex in the southwestern Yangtze Block, South China (in Chinese). Earth Sci, 45: 3054–3069

Cui X Z, Wang J, Ren G M, Deng Q, Sun Z M, Ren F, Chen F L. 2020b. Paleoproterozoic tectonic evolution of the Yangtze Block: New evidence from ca. 2.36 to 2.22 Ga magmatism and 1.96 Ga metamorphism in the Cuoke complex, SW China. Precambrian Res, 337: 105525

Cui X Z, Wang J, Wang X C, Wilde S A, Ren G M, Li S J, Deng Q, Ren F, Liu J P. 2021. Early crustal evolution of the Yangtze Block: Constraints from zircon U-Pb-Hf isotope systematics of 3.1–1.9 Ga granitoids in the Cuoke Complex, SW China. Precambrian Res, 357: 106155

Dong C, Xie H, Kröner A, Wang S, Liu S, Xie S, Song Z, Ma M, Liu D, Wan Y. 2017. The complexities of zircon crystllazition and overprinting during metamorphism and anatexis: An example from the late Archean TTG terrane of western Shandong Province, China. Precambrian Res, 300: 181–200

Gao S, Ling W, Qiu Y, Lian Z, Hartmann G, Simon K. 1999. Contrasting geochemical and Sm-Nd isotopic compositions of Archean metasediments from the Kongling high-grade terrain of the Yangtze craton: evidence for cratonic evolution and redistribution of REE during crustal anatexis. Geochim Cosmochim Acta, 63: 2071–2088

Gao S, Yang J, Zhou L, Li M, Hu Z, Guo J, Yuan H, Gong H, Xiao G, Wei J. 2011. Age and growth of the Archean Kongling terrain, South China, with emphasis on 3.3 Ga granitoid gneisses. Am J Sci, 311: 153–182

Griffin W L, Belousova E A, Shee S R, Pearson N J, O'Reilly S Y. 2004. Archean crustal evolution in the northern Yilgarn Craton: U-Pb and Hf-isotope evidence from detrital zircons. Precambrian Res, 131: 231–282

Griffin W L, Wang X, Jackson S E, Pearson N J, O'Reilly S Y, Xu X, Zhou X. 2002. Zircon chemistry and magma mixing, SE China: *In-situ* analysis of Hf isotopes, Tonglu and Pingtan igneous complexes. Lithos, 61: 237–269

Guo J L, Gao S, Wu Y B, Li M, Chen K, Hu Z C, Liang Z W, Liu Y S, Zhou L, Zong K Q, Zhang W, Chen H H. 2014. 3.45 Ga granitic gneisses from the Yangtze Craton, South China: Implications for Early Archean crustal growth. Precambrian Res, 242: 82–95

Guo J L, Wu Y B, Gao S, Jin Z M, Zong K Q, Hu Z C, Chen K, Chen H H, Liu Y S. 2015. Episodic Paleoarchean-Paleoproterozoic (3.3–2.0 Ga) granitoid magmatism in Yangtze Craton, South China: Implications for late Archean tectonics. Precambrian Res, 270: 246–266

Han P Y, Guo J L, Chen K, Huang H, Zong K Q, Liu Y S, Hu Z C, Gao S. 2017a. Widespread Neoarchean (~2.7–2.6 Ga) magmatism of the Yangtze craton, South China, as revealed by modern river detrital zircons. Gondwana Res, 42: 1–12

Han Q, Peng S, Kusky T, Polat A, Jiang X, Cen Y, Liu S, Deng H. 2017b. A Paleoproterozoic ophiolitic mélange, Yangtze craton, South China: Evidence for Paleoproterozoic suturing and microcontinent amalgamation. Precambrian Res, 293: 13–38

Han Q, Peng S, Polat A, Kusky T, Deng H, Wu T. 2018. A ca. 2.1 Ga Andean-type margin built on metasomatized lithosphere in the northern Yangtze craton, China: Evidence from high-Mg basalts and andesites. Precambrian Res, 309: 309–324

Han Q, Peng S. 2020. Paleoproterozoic subduction within the Yangtze Craton: Constraints from Nb-enriched mafic dikes in the Kongling complex. Precambrian Res, 340: 105634

Hu J, Liu X C, Chen L Y, Qu W, Li H K, Geng J Z. 2013. A ~2.5 Ga magmatic event at the northern margin of the Yangtze craton: Evidence from U-Pb dating and Hf isotope analysis of zircons from the Douling Complex in the South Qinling orogen. Chin Sci Bull, 58: 3564–3579

Hu Z C, Liu Y S, Gao S, Liu W G, Zhang W, Tong X R, Lin L, Zong K Q, Li M, Chen H H, Zhou L, Yang L. 2012. Improved *in situ* Hf isotope ratio analysis of zircon using newly designed X skimmer cone and jet sample cone in combination with the addition of nitrogen by laser ablation multiple collector ICP-MS. J Anal At Spectrom, 27: 1391–1399

Huang M D, Cui X Z, Ren G M, Guo J W, Ren F, Pang W H, Cheng F L. 2020. The 2.73 Ga I-type granites in the Lengshui Complex and implications for the Neoarchean tectonic evolution of the Yangtze Craton. Int Geol Rev, 62: 649–664

Hui B, Dong Y P, Cheng C, Long X P, Liu X M, Yang Z, Sun S S, Zhang F F, Varga J. 2017. Zircon U-Pb chronology, Hf isotope analysis and whole-rock geochemistry for the Neoarchean-Paleoproterozoic Yudongzi complex, northwestern margin of the Yangtze craton, China. Precambrian Res, 301: 65–85

Iizuka T, Yamaguchi T, Hibiya Y, Amelin Y. 2015. Meteorite zircon constraints on the bulk Lu-Hf isotope composition and early differentiation of the Earth. Proc Natl Acad Sci USA, 112: 5331–5336

Jiao W F, Wu Y B, Yang S H, Peng M, Wang J. 2009. The oldest basement rock in the Yangtze Craton revealed by zircon U-Pb age and Hf isotope composition. Sci China Ser D-Earth Sci, 52: 1393–1399

King E M, Valley J W, Davis D W, Edwards G R. 1998. Oxygen isotope ratios of Archean plutonic zircons from granite-greenstone belts of the Superior Province: Indicator of magmatic source. Precambrian Res, 92: 365–387

Laurent O, Martin H, Moyen J F, Doucelance R. 2014. The diversity and evolution of late-Archean granitoids: Evidence for the onset of "modern-style" plate tectonics between 3.0 and 2.5 Ga. Lithos, 205: 208–235

Lei N Z, Wu Y B. 2008. Zircon U-Pb age, trace element, and Hf isotope evidence for Paleoproterozoic granulite-facies metamorphism and Archean crustal remnant in the Dabie Orogen. J China Univ Geosci, 19: 110–134

Li J Y, Wang X L, Wang D, Du D H, Yu J H, Gu Z D, Huang Y, Li L S. 2021. Pre-Neoproterozoic continental growth of the Yangtze Block: From continental rifting to subduction-accretion. Precambrian Res, 355: 106081

Li L, Lin S, Davis D W, Xiao W, Xing G, Yin C. 2014. Geochronology and geochemistry of igneous rocks from the Kongling terrane: Implications for Mesoarchean to Paleoproterozoic crustal evolution of the Yangtze Block. Precambrian Res, 255: 30–47

Li X H, Tang G Q, Gong B, Yang Y H, Hou K J, Hu Z C, Li Q L, Liu Y, Li W X. 2013. Qinghu zircon: A working reference for microbeam analysis of U-Pb age and Hf and O isotopes. Chin Sci Bull, 58: 4647–4654

Li Y H, Zheng J P, Ping X Q, Xiong Q, Xiang L, Zhang H. 2018. Complex growth and reworking processes in the Yangtze cratonic nucleus. Precambrian Res, 311: 262–277
Ling W L, Duan R C, Liu X M, Cheng J P, Mao X W, Peng L H, Liu Z X, Yang H M, Ren B F. 2010. U-Pb dating of detrital zircons from the Wudangshan Group in the South Qinling and its geological significance. Chin Sci Bull, 55: 2440–2448
Liou J G, Ernst W G, Zhang R Y, Tsujimori T, Jahn B M. 2009. Ultrahigh-pressure minerals and metamorphic terranes—The view from China. J Asian Earth Sci, 35: 199–231
Liu B, Zhai M G, Zhao L, Cui X H, Zhou L G. 2019. Zircon U-Pb-Hf isotope studies of the early Precambrian metasedimentary rocks in the Kongling terrane of the Yangtze Block, South China. Precambrian Res, 320: 334–349
Liu C R, Xu D L, Zhao X M, Deng X, Tang M T. 2021. Depositional age and provenance of metasedimentary rocks in the Qichun tectonic mélange, southern Dabie orogen (in Chinese). South China Geol, 37: 1–28
Liu H, Xia B, Zhang Y. 2004. Zircon SHRIMP dating of sodium alkaline rocks from Maomaogou area of Huili County in Panxi, SW China and its geological implications. Chin Sci Bull, 49: 1750–1756
Liu X M, Gao S, Diwu C R, Ling W L. 2008. Precambrian crustal growth of Yangtze Craton as revealed by detrital zircon studies. Am J Sci, 308: 421–468
Liu Y S, Gao S, Hu Z C, Gao C G, Zong K Q, Wang D B. 2010. Continental and oceanic crust recycling-induced melt-peridotite interactions in the Trans-North China Orogen: U-Pb dating, Hf isotopes and trace elements in zircons from mantle xenoliths. J Petrol, 51: 537–571
Liu Y S, Hu Z C, Gao S, Günther D, Xu J, Gao C G, Chen H H. 2008. *In situ* analysis of major and trace elements of anhydrous minerals by LA-ICP-MS without applying an internal standard. Chem Geol, 257: 34–43
Ludwig K R. 2003. User's Manual for Isoplot 3.00, a Geolochronolgical Toolkit for Microsoft Excel. Berkeley Geochronol Center Spec Publ, 4: 25–32
Maruyama S, Santosh M, Azuma S. 2018. Initiation of plate tectonics in the Hadean: Eclogitization triggered by the ABEL Bombardment. Geosci Front, 9: 1033–1048
Nam T N, Toriumi M, Sano Y, Terada K, Thang T T. 2003. 2.9, 2.36, and 1.96 Ga zircons in orthogneiss south of the Red River shear zone in Viet Nam: Evidence from SHRIMP U-Pb dating and tectonothermal implications. J Asian Earth Sci, 21: 743–753
Qiu X F, Deng X, Jiang T, Xu Q, Yang W W. 2021b. First discovery of Hadean xenocrystal zircons from granitic gneisses in the northern Dabie orogen. Acta Geol Sin, 95: 1775–1776
Qiu X F, Jiang T, Wu N W, Zhao X M, Xu Q. 2020. Neoarchean crustal rocks and Paleoproterozoic migmatization in the Dabie orogen: Evidence from zircon U-Pb age and Hf isotopes (in Chinese). Acta Geol Sin, 94: 729–738
Qiu X F, Tong X R, Jiang T, Khattak N U. 2021a. Reworking of Hadean continental crust in the Dabie orogen: Evidence from the Muzidian granitic gneisses. Gondwana Res, 89: 119–130
Qiu X F, Yang H M, Zhao X M, Lu S S, Jiang T, Duan R C, Liu C P, Peng L H, Wei Y X. 2019. Neoarchean granitic gneisses in the Kongling Complex, Yangtze Craton: Petrogenesis and tectonic implications (in Chinese). Earth Sci, 44: 415–426
Qiu Y M, Gao S, McNaughton N J, Groves D I, Ling W L. 2000. First evidence of >3.2 Ga continental crust in the Yangtze craton of south China and its implications for Archean crustal evolution and Phanerozoic tectonics. Geology, 28: 11–14
Satkoski A M, Fralick P, Beard B L, Johnson C M. 2017. Initiation of modern-style plate tectonics recorded in Mesoarchean marine chemical sediments. Geochim Cosmochim Acta, 209: 216–232
Söderlund U, Patchett P J, Vervoort J D, Isachsen C E. 2004. The ^{176}Lu decay constant determined by Lu-Hf and U-Pb isotope systematics of Precambrian mafic intrusions. Earth Planet Sci Lett, 219: 311–324
Sun M, Chen N, Zhao G, Wilde S A, Ye K, Guo J, Chen Y, Yuan C. 2008. U-Pb zircon and Sm-Nd isotopic study of the Huangtuling granulite, Dabie-Sulu belt, China: Implication for the paleoproterozoic tectonic history of the Yangtze Craton. Am J Sci, 308: 469–483
Sun S S, McDonough W F. 1989. Chemical and isotopic systematics of oceanic basalts: Implications for mantle composition and processes. Geol Soc Lond Spec Publ, 42: 313–345
Tu C, Zhang S B, Su K, Liang T. 2021. Zircon U-Pb Dating and Lu-Hf Isotope Results for Feidong Complex: Implications for Coherent Basement of the Yangtze Craton (in Chinese). Earth Sci, 46: 1630–1643
Valley J W, Kinny P D, Schulze D J, Spicuzza M J. 1998. Zircon megacrysts from kimberlite: Oxygen isotope variability among mantle melts. Contrib Mineral Petrol, 133: 1–11
Wan Y S, Ma M Z, Dong C Y, Xie H Q, Xie S W, Ren P, Liu D Y. 2015. Widespread late Neoarchean reworking of Meso- to Paleoarchean continental crust in the Anshan-Benxi area, North China Craton, as documented by U-Pb-Nd-Hf-O isotopes. Am J Sci, 315: 620–670
Wang K, Dong S, Li Z X, Han B. 2018. Age and chemical composition of Archean metapelites in the Zhongxiang Complex and implications for early crustal evolution of the Yangtze Craton. Lithos, 320-321: 280–301
Wang W, Cawood P A, Pandit M K, Zhou M F, Chen W T. 2017. Zircon U-Pb age and Hf isotope evidence for an Eoarchaean crustal remnant and episodic crustal reworking in response to supercontinent cycles in NW India. J Geol Soc, 174: 759–772
Wang W, Cawood P A, Zhou M F, Zhao J H. 2016. Paleoproterozoic magmatic and metamorphic events link Yangtze to northwest Laurentia in the Nuna supercontinent. Earth Planet Sci Lett, 433: 269–279
Wang Z J, Wang J, Du Q D, Deng Q, Yang F, Wu H. 2013. Mature Archean continental crust in the Yangtze craton: Evidence from petrology, geochronology and geochemistry. Chin Sci Bull, 58: 2360–2369
Wang Z, Deng Q, Duan T, Yang F, Du Q, Xiong X, Liu H, Cao B. 2018. 2.85 Ga and 2.73 Ga A-type granites and 2.75 Ga trondhjemite from the Zhongxiang Terrain: Implications for early crustal evolution of the Yangtze Craton, South China. Gondwana Res, 61: 1–19
Wang Z, Wang J, Deng Q, Du Q, Zhou X, Yang F, Liu H. 2015. Paleoproterozoic I-type granites and their implications for the Yangtze block position in the Columbia supercontinent: Evidence from the Lengshui Complex, South China. Precambrian Res, 263: 157–173
Wang W, Zhao J H, Zhou M F, Pandit M K, Zheng J P. 2018. Depositional age, provenance characteristics and tectonic setting of the Meso- and Neoproterozoic sequences in SE Yangtze Block, China: Implications on Proterozoic supercontinent reconstructions. Precambrian Res, 309: 231–247
Wei J Q, Wei Y X, Wang J X, Wang X D. 2020. Geochronological constraints on the formation and evolution of the Huangling basement in the Yangtze craton, South China. Precambrian Res, 342: 105707
Wei Y X, Zhou W X, Hu Z X, Li H Q, Huang X X, Zhao X M, Xu D L. 2019. Geochronology and geochemistry of Archean TTG and tremolite schist xenoliths in yemadong complex: Evidence for ≥3.0 Ga Archean continental crust in kongling high-grade metamorphic terrane, Yangtze Craton, China. Minerals, 9: 689
Wu Y B, Chen D G, Xia Q K, Deloule E, Cheng H. 2002. SIMS U-Pb dating of zircons in granulite of Huangtuling from Northern Dabieshan (in Chinese). Acta Petrol Sin, 18: 378–382
Wu Y B, Chen D G, Zheng Y F, Xia Q K, Tu X L. 2004. Trace element geochemistry of zircons in migmatitic gneiss at Manshuihe, North Dabieshan and its geological implications (in Chinese). Acta Petrol Sin, 20: 152–161
Wu Y B, Tang J, Zhang S B, Zhao Z F. 2007. SHRIMP zircon U-Pb dating for two episodes of migmatization in the Dabie orogen. Chin Sci Bull, 52: 1836–1842
Wu Y B, Zheng Y F, Gao S, Jiao W F, Liu Y S. 2008. Zircon U-Pb age and trace element evidence for Paleoproterozoic granulite-facies metamorphism and Archean crustal rocks in the Dabie Orogen. Lithos, 101: 308–322
Wu Y B, Zhou G Y, Gao S, Liu X C, Qin Z W, Wang H, Yang J Z, Yang S H. 2014. Petrogenesis of Neoarchean TTG rocks in the Yangtze Craton and its implication for the formation of Archean TTGs. Precambrian Res, 254: 73–86
Wu Y, Gao S, Zhang H, Zheng J, Liu X, Wang H, Gong H, Zhou L, Yuan

H. 2012. Geochemistry and zircon U-Pb geochronology of Paleoproterozoic arc related granitoid in the Northwestern Yangtze Block and its geological implications. Precambrian Res, 200-203: 26–37
Xia Q K, Zbeng Y F, Ge N J, Deloule E. 2003. U-Pb ages and oxygen isotope compositions of zircons from gneiss of Huangtuling, Northern Dabie: Old protolith and multi-stage evolution (in Chinese). Acta Petrol Sin, 19: 506–512
Yang Q, Xia X P, Zhang W F, Zhang Y Q, Xiong B Q, Xu Y G, Wang Q, Wei G J. 2018. An evaluation of precision and accuracy of SIMS oxygen isotope analysis. Solid Earth Sci, 3: 81–86
Yao J, Wang W, Liu S, Cawood P A, Niu P, Lu D, Guo L. 2020. Crust-mantle geodynamic origin of ~2.7 Ga granitoid diversification in the Jiaobei terrane, North China Craton. Precambrian Res, 346: 105821
Yin C, Lin S, Davis D W, Zhao G, Xiao W, Li L, He Y. 2013. 2.1–1.85 Ga tectonic events in the Yangtze Block, South China: Petrological and geochronological evidence from the Kongling Complex and implications for the reconstruction of supercontinent Columbia. Lithos, 182-183: 200–210
Zhang Q Q, Gao X Y, Zhang S B, Zheng Y F. 2020. Paleoproterozoic tectonic evolution of the northern Yangtze craton from oceanic subduction through continental collision to continental rifting: Geochronological and geochemical records of metabasites from the Tongbai orogen in central China. Precambrian Res, 350: 105920
Zhang Q, Zhai M G. 2012. What is the Archean TTG? (in Chinese). Acta Petrol Sin, 28: 3446–3456
Zhang S B, Zheng Y F, Wu P, He Q, Rong W, Fu B, Yang Y H, Liang T. 2020. The nature of subduction system in the Neoarchean: Magmatic records from the northern Yangtze Craton, South China. Precambrian Res, 347: 105834
Zhang S B, Zheng Y F, Wu Y B, Zhao Z F, Gao S, Wu F Y. 2006a. Zircon U-Pb age and Hf-O isotope evidence for Paleoproterozoic metamorphic event in South China. Precambrian Res, 151: 265–288
Zhang S B, Zheng Y F, Wu Y B, Zhao Z F, Gao S, Wu F Y. 2006b. Zircon U-Pb age and Hf isotope evidence for 3.8 Ga crustal remnant and episodic reworking of Archean crust in South China. Earth Planet Sci Lett, 252: 56–71
Zhang S B, Zheng Y F. 2013. Formation and evolution of Precambrian continental lithosphere in South China. Gondwana Res, 23: 1241–1260
Zhang S B, Zheng Y F. 2007. Growth and reworking of the Yangtze continental nucleus: Evidence from zircon U-Pb ages and Hf isotopes (in Chinese). Acta Petrol Sin, 23: 393–402
Zhang Z, Zhang G, Tang S, Beijing, An X. 2001. On the age of metamorphic rocks of the Yudongzi Group and the Archean crystalline basement of the Qinling Orogen. Acta Geol Sin, 12: 739–773
Zhao T, Cawood P A, Wang K, Zi J W, Feng Q, Nguyen Q M, Tran D M. 2019. Neoarchean and Paleoproterozoic K-rich granites in the Phan Si Pan Complex, north Vietnam: Constraints on the early crustal evolution of the Yangtze Block. Precambrian Res, 332: 105395
Zhao T, Li J, Liu G, Cawood P A, Zi J W, Wang K, Feng Q, Hu S, Zeng W, Zhang H. 2020. Petrogenesis of Archean TTGs and potassic granites in the southern Yangtze Block: Constraints on the early formation of the Yangtze Block. Precambrian Res, 347: 105848
Zhao T, Zhu G, Wu Q, Hu R, Wu Y, Xu Z, Ye J. 2021. Evidence for discrete Archean microcontinents in the Yangtze Craton. Precambrian Res, 361: 106259
Zheng J, Griffin W L, O′Reilly S Y, Zhang M, Pearson N, Pan Y. 2006. Widespread Archean basement beneath the Yangtze craton. Geology, 34: 417–420
Zheng Y F. 2012. Metamorphic chemical geodynamics in continental subduction zones. Chem Geol, 328: 5–48
Zheng Y F, Zhang S B. 2007. Formation and evolution of Precambrian continental crust in South China. Chin Sci Bull, 52: 1–12
Zheng Y F, Zhou J B, Wu Y B, Xie Z. 2005. Low-grade metamorphic rocks in the Dabie-Sulu orogenic belt: A passive-margin accretionary wedge deformed during continent subduction. Int Geol Rev, 47: 851–871
Zheng Y F, Zhao Z F, Chen R X. 2019. Ultrahigh-pressure metamorphic rocks in the Dabie-Sulu orogenic belt: Compositional inheritance and metamorphic modification. Geol Soc Lond Spec Publ, 474: 89–132
Zhou G Y, Wu Y B, Gao S, Yang J Z, Zheng J P, Qin Z W, Wang H, Yang S H. 2015. The 2.65 Ga A-type granite in the northeastern Yangtze craton: Petrogenesis and geological implications. Precambrian Res, 258: 247–259
Zhou G Y, Wu Y B, Li L, Zhang W X, Zheng J P, Wang H, Yang S H. 2018. Identification of ca. 2.65 Ga TTGs in the Yudongzi complex and its implications for the early evolution of the Yangtze Block. Precambrian Res, 314: 240–263
Zhou K, Chen Y X, Zhang S B, Zheng Y F. 2020. Zircon evidence for the Eoarchean (~3.7 Ga) crustal remnant in the Sulu Orogen, eastern China. Precambrian Res, 337: 105529
Zhou W, Huang B, Wei Y, Li H, Tan M, Fu D. 2021. Paleoproterozoic ophiolitic mélanges and orogenesis in the northern Yangtze Craton: Evidence for the operation of modern-style plate tectonics. Precambrian Res, 364: 106385
Zong K, Klemd R, Yuan Y, He Z, Guo J, Shi X, Liu Y, Hu Z, Zhang Z. 2017. The assembly of Rodinia: The correlation of early Neoproterozoic (ca. 900 Ma) high-grade metamorphism and continental arc formation in the southern Beishan Orogen, southern Central Asian Orogenic Belt (CAOB). Precambrian Res, 290: 32–48

(Responsible editor: Yongfei ZHENG)